Studies into the structure and motion of density currents. September 1983.

Author:
Wilkinson, D. L.

Publication details:
Commissioning Body: State Pollution Control Commission of N.S.W.
Report No. UNSW Water Research Laboratory Report No. 160
0858242915 (ISBN)

Publication Date:
1983

DOI:
https://doi.org/10.4225/53/57983d4acf9e0

THE UNIVERSITY OF NEW SOUTH WALES
water research laboratory
Manly Vale N.S.W. Australia

STUDIES INTO THE STRUCTURE AND MOTION OF DENSITY CURRENTS

by
D.L. Wilkinson

Research Report No. 160
1983

STUDIES INTO THE STRUCTURE AND MOTION OF DENSITY CURRENTS

BY

D.L. WILKINSON

https://doi.org/10.4225/53/57983d4acf9e0

REPORT NO. 160

SEPTEMBER, 1983

BIBLIOGRAPHIC DATA SHEET	1. REPORT No. 160	2. I.S.B.N. 0/85824/291/5

3. TITLE AND SUBTITLE

STUDIES INTO THE STRUCTURE AND MOTION OF DENSITY CURRENTS

4. REPORT DATE

SEPTEMBER 1983

5. AUTHOR (S)

D.L. WILKINSON

6. SPONSORING ORGANISATION

STATE POLLUTION CONTROL COMMISSION OF NEW SOUTH WALES and
THE UNIVERSITY OF NEW SOUTH WALES

7. SUPPLEMENTARY NOTES

8. ABSTRACT

The report describes in detail the frontal structure of the head of a density current and the nature of the layer behind the head. The descriptions are based on the results of laboratory experiments in which a dense saline layer flowed beneath a buoyant layer in a water tunnel. Data are presented on the volume and density fluxes, frontal celerity and the nature of the dissipative region behind the head for a range of fractional depths. The form drag associated with the head of a density current is also computed.

9. DISTRIBUTION STATEMENT

UNRESTRICTED

10. DESCRIPTORS

Density Currents ; Gravity Flow ; Density Stratification

11. IDENTIFIERS

12. CLASSIFICATION	13. NUMBER OF PAGES 36 pages + 23 figures	14. PRICE $30

CONTENTS

This report contains the results of a study into the behaviour of density or gravity current propagating over horizontal and gently inclined surfaces. Both the internal structure of the density currents and their bulk behaviour were investigated.

The study was undertaken with the assistance of a grant from the State Pollution Control Commission of New South Wales. The receipt of this grant is gratefully acknowledged.

The author would also like to thank the staff of the Water Research Laboratory, in particular the workshop staff without whose help this study would not have been possible.

STUDIES INTO THE STRUCTURE AND MOTION OF DENSITY CURRENTS

BY D.L. WILKINSON

1. INTRODUCTION

The terms gravity current or density current are used to describe the motion of a wedge of heavy fluid as it intrudes into an expanse of lighter fluid. Many such flows occur naturally and take the form of sea breeze fronts (Simpson, 1969), intrusions into water storage reservoirs (Herbert et al 1979) or turbidity currents (Keunen, 1952). A gravity current can also be lighter than the surrounding fluid. For example, cooling water carrying waste heat from a power station forms a density current at the surface when it is discharged into a cooling pond. The motion of methane along the roofs of mine shafts is another example.

Density currents are created when density differences produce horizontal gradients in the hydrostatic pressure. These pressure gradients are usually balanced by the inertia of the resulting fluid motions and by friction. The density differences which provide the forcing for density currents are typically one to four orders of magnitude less than the density of either fluid. Provided the density current and the surrounding fluid are miscible, and their density difference is at least two orders of magnitude less than their densities (which applies to all the examples quoted previously) the general structure of the flow will be independent of the actual density ratio of the two fluids. Benjamin (1968) in a very comprehensive treatment of nonmiscible density currents pointed out that the motion of a gravity current in which the densities of the two fluids differed by orders of magnitude, for example an air cavity intruding into a water tunnel, was dynamically similar to a flow in which the two fluids were of nearly the same density. Benjamin also demonstrated that the proximity of horizontal boundaries would have a significant effect on the speed of a density current and the rate of energy dissipation associated with the flow.

This report describes an experimental study into the structure of the frontal region of density currents travelling along horizontal surfaces. The influence of a confining upper boundary on the motion and structure of

a density current is examined in some detail.

The report commences with a brief description of the basic structure of the frontal region and this is followed by a review of earlier theoretical and experimental studies. The experimental facility and techniques employed in the present study are then described and scaling parameters defined.

A detailed description and analysis of the experimental data follows commencing with normalised density and velocity profiles for density currents moving beneath deep and shallow ambient layers. The stability of the sheared region of the following layer is discussed and the variation of the normalised fluxes of density and volume with distance from the head of the density current is examined.

The physical implications of the various definitions of the following layer depth are considered and the influence of the ratio of this depth to the distance between confining boundaries on the motion of the head is analysed. Finally the structure of the wake which forms in the lee of the head is examined. It is found that buoyancy effects within the wake are negligible and the wake does not collapse as has been commonly accepted in earlier work.

2. BASIC STRUCTURE OF THE FRONTAL REGION

Figure 1(a) is a photograph of the frontal region of a density current moving between horizontal upper and lower boundaries. The density current has been dyed and contrasts against the clear ambient fluid it displaces. Figure 1(b) is a shadowgraph of the same flow without the dye and gives some idea of mixing regions associated with the flow. Figure 2 is a sketch of the flow in which various regions have been identified.

The photographs reveal a bulbous head at the front of the dense layer which is characteristic of all density currents moving beneath deep ambient fluid. The leading edge or nose of the front rides some distance above the floor and Simpson (1972) showed that some ambient fluid was over-ridden by the density current and was entrained up into head from below.

Although the dyed flow in Figure 1(a) has an apparently streamlined head, Figure 1(b) shows that the head is highly turbulent. Kelvin-Helmholtz instabilities develop from near the front of the head and degenerate into characteristic turbulent billows immediately behind the head. The diameter of the billows is comparable with the height of the head. The billows are clearly visible in both the dyed density current and in the shadowgraph. Ambient fluid is entrained into the billows which subsequently collapse to form a stratified wake behind the head.

Downstream of the head four regions can be identified, a nearly homogeneous dense layer adjacent to the lower boundary, a highly stratified shear layer, a turbulent wake and finally the upper layer consisting of displaced ambient fluid.

Velocities in the dense homogeneous layer, above the bottom boundary layer, exceed the celerity of the front. Thus a net circulation exists from the dense bottom layer to the stratified shear layer above. A vertical flow exists at the very nose of the density current. It is important to note that the depth of the dense layer is not constant, as has often been assumed, but increases with distance from the head. Two factors contribute to this non-uniformity. Firstly friction at the lower boundary and secondly longitudinal non-uniformities in the wake and stratified shear layer above the dense homogeneous layer.

The stratified shear layer is characterised by strong vertical density gradients and high fluid shear. There is pronounced suppression of turbulence by gravity at the bottom of this layer. The thickness of the shear layer is comparable with the thickness of the dense layer below and decreases with distance from the front.

Above the stratified shear layer is a homogeneous shear layer which forms the wake behind the head of the density current. Close to the head flow this region is highly three-dimensional and billows, produced by Kelvin-Helmholtz instability behind the head, can be detected in the shadowgraphs because of wisps of dense fluid entrained into them. Gravitational collapse of the stratified shear region gives the impression that the wake region also collapses. Observations of vertical dye traces during the passage of a density current showed that the thickness of wake increased with distance behind the head until its growth was ultimately limited by the proximity of the upper boundary.

The upper most layer is basically a potential flow induced by the intrusion of the density current. The momentum induced in this layer reduces as the depth of the upper layer is increased. Consequently, for a given flux of dense fluid the celerity of the front increases as the upper boundary becomes more distant.

3. MOTION OF THE FRONT - THEORETICAL REVIEW

Von Karman (1940) was the first investigator to quantify the motion of a density current front. Von Karman visualised the flow to be as shown in Figure 3. He assumed the flow to be steady when viewed in a frame of reference moving with the front, and that some distance downstream of the front, the streamlines became parallel and the pressure hydrostatic. Von Karman applied the Bernoulli equation along the streamline A.B.D equating the values of the Bernoulli constant at the stagnation point B and above the uniformly flowing layer at C to get:

$$p_B = \frac{\rho_1 c^2}{2} + p_D + \rho_1 gh \qquad (1)$$

where $p_{B,D}$ = pressure at points B and D respectively

ρ_1 = density of the lighter fluid

c = celerity of the front

and h = depth of the uniform layer behind the head

von Karman assumed that the pressure distribution inside the front was hydrostatic, that is that velocities within the gravity current were essentially parallel, and was able to relate p_B and p_D by the relationship:-

$$p_B = p_D + \rho_2 gh \qquad (2)$$

where ρ_2 is the density of the denser fluid.

Elimination of p_B between (1) and (2) leads to an expression for the speed of the front:

$$c = \left[\frac{2(\rho_2 - \rho_1)gh}{\rho_1}\right]^{0.5} \qquad (3)$$

Benjamin (1968) has criticised von Karman's deviation in that the Bernoulli equation was applied along a streamline which traverses a region of high turbulence behind the head of the density current. Benjamin adopted a more fundamental approach and examined the balance of flow force (the sum of the depth integrated momentum and pressure) at sections upstream and downstream of the density current head. Surprisingly, Benjamin obtained the same result as von Karman for the case of a density current moving beneath a deep ambient layer.

Benjamin assumed that the density current intruded with celerity c into an ambient fluid which remained at rest at large distances in front of the moving dense layer. The ambient fluid was confined by a horizontal boundary at height H above the bottom boundary which was also assumed to be horizontal. The flow is shown schematically in Figure 4. The flow force at sections upstream and downstream of the head were equated to give (4) below.

$$\frac{\rho_1 gH^2}{2} + \rho_1 c^2 H = \frac{\rho_1 gH^2}{2} + \frac{(\rho_2-\rho_1)gh^2}{2} + \rho_1 u^2(H-h) + \delta pH = 0 \qquad (4)$$

in which u = velocity in the upper layer behind the front

and $\delta p = p_E - p_F$ = pressure differential between points E and F on the upper boundary far downstream and far upstream of the front respectively.

If H, h, ρ_1, ρ_2 and g are taken as the independent variables then c, u and δp remain as the independent variables and two further relationships are required for a solution. Continuity enables u to be eliminated since

$$cH = u(H - h) \qquad (5)$$

Benjamin followed von Karman and assumed B to be a stagnation point and that pressure distribution in the density current was hydrostatic. More specifically, they assumed that the pressure is constant along the bottom boundary of the density current. The unknown pressure change across the front δp can now be expressed in terms of the stagnation pressure by

applying the Bernoulli equation between A and B. Benjamin argued that use of the Bernoulli equation here was valid because experiments revealed no obvious energy dissipation between these points. Hence from the Bernoulli equation:

$$\frac{\rho_1 c^2}{2} = p_B - p_A \tag{6a}$$

However $p_F = p_A - \rho_1 gH$ (6b)

While $p_E = p_C - \rho_1 gH - (\rho_2-\rho_1)gh$ (6c)

Subtracting (6b) from (6c) and substituting $p_B = p_C$

$$p_E - p_F = \delta p = \frac{\rho_1 c^2}{2} - (\rho_2-\rho_1)gh \tag{7}$$

Equations 4,5 and 7 can be solved and the normalised celerity of the gravity current $c/\sqrt{[(\rho_2-\rho_1)gH/\rho_1]}$ is found to depend on the ratio of the current depth h to the distance between the confining boundaries H.

This relationship is given by:-

$$\frac{c}{\sqrt{(\Delta gH)}} = \left[\frac{\phi(1-\phi)(2-\phi)}{(1+\phi)}\right]^{0.5} \tag{8}$$

where $\Delta = \frac{\rho_2-\rho_1}{\rho_1}$ = density difference ratio

and ϕ = fractional layer depth = h/H

It will be noted that real solutions exist for the full range of fractional depths ($0 \leq \phi \leq 1$). Benjamin next examined the change in head f along the streamline E F as it traversed the head. Applying the Bernoulli equation at points E and F on this streamline yielded the following equation:

$$\frac{\rho_1 c^2}{2} + p_F = \frac{\rho_1 u^2}{2} + p_E + \rho_1 gf$$

Eliminating p_F and p_E using (7) and substituting for u using Equation (5) gives:-

$$\frac{f}{\Delta H} = \frac{\phi^2(1-2\phi)}{2(1-\phi^2)} \qquad (9)$$

Equations 8 and 9 are plotted in Figure 5. It will be noted that fractional depths greater than 0.5 involve an energy gain and therefore cannot be physically realised. It will also be noted that for values of the fractional depth between 0.219 and 0.500 two values of fractional depth are possible for a given front celerity. Benjamin showed that the smaller of these depths represented subcritical flow in the displaced upper layer while the larger fractional depth represented supercritical flow in the upper layer. It was argued that the supercritical regime was unstable and therefore the fractional depths were restricted to values between zero and 0.347.

As already mentioned the flow structure in Benjamin's model is highly idealised and viscous effects are ignored. Benjamin suggested that the motion of an air cavity into a long duct would be well described by his theory, however more recent work by Wilkinson (1982) has shown that in the range of fractional depths between 0.219 and 0.500 (the region where alternative depths existed in the steady model) the flow is unsteady, and Benjamin's steady model no longer applies. Benjamin's model is therefore only valid for air cavities when the fractional depths are between zero and 0.219 and for the energy conserving flow when $h/H = 1/2$.

Benjamin points out that as the fraction depth becomes very small the assumption that the flow is uniform far downstream of the front is unrealistic and hence the model cannot be expected to give accurate predictions of gravity current celerity when the overlying layer is relatively deep.

The normalised celerity of the density current front given by (8) can also be expressed in term of the depth of the following layer h rather that the distance between the confining boundaries H and is given by:

$$F = \frac{c}{\sqrt{(\Delta g h)}} = \left[\frac{(1-\phi)(2-\phi)}{1+\phi}\right]^{0.5} \qquad (10)$$

where F is the Froude number of the front.

Equation 10 is plotted in Figure 6 where it can be seen the frontal Froude number has a maximum value of $\sqrt{2}$ when the fractional depth is small and reduces to $1/\sqrt{2}$ when $\phi = 1/2$. However, according to Benajamin the

maximum value of ϕ which can be physically achieved is 0.347 which on substitution into Equation 7 gives F = 0.895.

The rate of energy dissipation associated with a density current (D) must be evaluated from a frame of reference in which the flow is steady (i.e. a frame which moves with the head). The flow passing over the now stationary head cH experiences a loss in head f (energy per unit weight of fluid) so the D = ρgcHf. As this energy is principally dissipated in the wake which develops behind the head it is interesting to compare it with the energy flux associated with the intruding density current (P). P is given by:

$$P = \rho ch \left(\frac{c^2}{2} + \Delta gh\right) = \tfrac{1}{2} \rho c \, \Delta g h^2 \, (2 + F^2)$$

The ratio of the rate of energy dissipation compared with the energy flux associated with the density current can be expressed in terms of the fractional depth after substitutions are made for f and F^2 using (9) and (10) respectively. The ratio is then given by:

$$\frac{D}{P} = \frac{1 - 2\phi}{(1 - \phi)(4 - \phi + \phi^2)} \qquad (11)$$

and it will be noted that as $\phi \to 0$, D/P $\to$ 1/4. Equation 11 is plotted in Figure 6. It can be seen that the rate of energy dissipation relative to the net energy flux increases as the fractional depth becomes smaller. This would imply that thickness of the wake behind the head and therefore the height of the head itself must increase relative to the depth of the following layer as the fractional depth becomes smaller.

Wilkinson and Wood (1972) collected available experimental data to show that fractional depth indeed does have a significant effect on the celerity of gravity current fronts. The lock exchange experiments Yih (1965) and Barr (1966) showed that for a nominal fractional depth of 1/2 the Froude number of the front was 0.67 and 0.65 respectively. These values compare favourably with Benjamin's value of $1/\sqrt{2}$ or 0.71. Other experiments with much smaller values of the fractional depth (typically $0.1 < \phi < 0.2$) by Keulegan (1958), Wood (1965) and Middleton (1966) gave a mean Froude number of 1.1 compared with Benjamin's values of 1.25 to 1.10 over a similar range of fractional depths.

Wilkinson and Wood showed that boundary conditions imposed on the motion of the ambient fluid in density current experiments has a significant influence on the motion of a density current front. The effect must

be considered when designing laboratory experiments. Three possible configurations are shown in Figure 7. Relative to the front the flow in all three experiments would be identical however, because of the differing boundary conditions restricting the flow of the ambient fluid, the velocity of the front would appear different to a stationary observed in all three configurations. This effect becomes more pronounced at larger values of the fractional depth. Wilkinson and Wood showed that for a fractional depth of 1/2 the Froude Number of the cavity front would have a value of $1/\sqrt{2}$ for the geometry shown in Figure 7(a) and a value of $\sqrt{2}$ for the geometry of Figure 7(c). The motion of the front in Figure 7(b) would be unsteady, corresponding initially to that shown in Figure 7(c) and finally to that shown in Figure 7(a) as the density front reached the end of the tank. The situation in Figure 1(b) might well apply to conditions in a lock separating fresh river water from saline ocean water. Denton et al (1981) demonstrated the importance of boundary configuration in their experiments with density intrusions in reservoirs.

Britter and Simpson (1978) have extended Benjamin's analysis by allowing for non-uniform velocity and density distributions in the layer following behind the head. This is accomplished by the introduction of a stratified shear layer between homogeneous upper and lower layers. Their schematisation is shown in Figure 8. The density current is regarded as being confined to the lowest uniform density layer and consequently the velocity in this layer must exceed the velocity of the front so that dense fluid can be supplied to the shear layer. Thereby a further variable, the circulating flow $Q = u_4 h_4$ is introduced into the analysis. Empirically derived functions were fitted for u and $(\rho-\rho_1)/\rho_1$ in the sheared region and substitution into the flow force equation resulted in the plot shown in Figure 9 for the frontal Froude number $F = c/\sqrt{gh_4}$ versus the fractional depth h_4/H for various values of the circulation parameter $q = \Delta gQ/c^3$

The lower shaded area denotes a region where no physical solutions exist as the flow force balance would require the circulation parameter to be negative. The upper shaded region denotes negative values of the upper layer depth h_2 and also does not represent physically realisable solutions. Thus meaningful solutions are restricted to a narrow band of celerities except when the fractional depth is very small. Both Britter and Simpson and Benjamin point out that uniform flow assumption in the upper layer becomes tenuous when this layer is very deep.

Britter and Simpson also argued that if the flow is not to be controlled by the source configuration then the celerity of long interfacial waves relative to the head must be zero or to the right in Figure 8 in which case, in the absence of the mixed region,

$$\frac{U_2^2}{g'h_2} + \frac{U_4^2}{g'h_4} \leq 1. \qquad (12)$$

The existence of the mixed region invalidates the physical basis of (12) however it can be reasonably assumed that

$$\frac{U_4}{\sqrt{(g'h_4)}} < 1$$

and this condition is shown by the dashed curve in Figure 9. Physically realisable solutions are confined to the region between the dashed curve and limiting condition of no internal circulation ($q = 0$) originally derived by Benjamin.

Britter and Simpson's model places a limit on the maximum entrainment which can occur in the frontal region. However only at very small values of the fractional depth was the observed entrainment comparable with the maximum possible entrainment.

Britter and Simpson's schematisation of the layer flowing behind the head, into a homogeneous layer of depth h_4, and a stratified shear layer of depth h_3 is somewhat arbitrary. As will be seen in the experiments to be described later, neither h_3 or h_4 is uniform with distance behind the head. Two factors contribute to this non-uniformity. Close to the front, gravity causes a collapse of the stratified shear layer so that h_3 reduces with distance from the head. The second factor is a result of friction at the lower boundary which requires that density surfaces (pynoclines) be inclined to the horizontal for the density flow to be maintained. Steady uniform flow of a density current over a horizontal surface cannot be realised in a viscous fluid.

In a subsequent paper (Simpson and Britter, 1979) the same authors presented a detailed analysis of the structure of the head of a density current advancing over a horizontal bottom. A facility in which a density current could be held stationary against an opposing flow was used to

obtain detailed density and velocity profiles in the layer immediately behind the head of the density current. Three dependent parameters, a frontal Froude number $c/(\Delta g h_4)^{1/2}$, the circulating flow parameter $\Delta g Q_c/c^2$ where $\left[Q_c = \int_0^{h_4} (u - c)dy\right]$, and the ratio of the depths of the stratified shear layer to the depth of the homogeneous layer $h_3//h_4$ were measured in a series of experiments and expressed in terms of the fractional depth $h_3//h_1$. The influence of Reynold's number on the flow was also discussed. A more detailed examination of their work will be postponed until a comparison can be made with the experiments described in this report.

Denton et al (1981) have recently described in detail, the density flows associated with the intrusion of dense, intrusive and buoyant layers into reservoirs. A typical reservoir geometry was modelled in a laboratory flume 20m wide, 40cm deep and having a working section 5m in length. The experiment commenced with a homogeneous flow through the system. The density of the inflow was then changed to a predetermined value at the same flow rate and the progress of the resulting density current was recorded. The data from these experiments is the most detailed of its type yet recorded in the literature. The experiments are restricted to relatively large volumes of the alternate depth.

Denton et al have introduced some new dimensionless variables with the intention of separating the dependent and independent variables associated with density flows into reservoirs. In particular a shallowness parameter q* is defined in terms of the volumetric flow rate per unit width (q), Δg and total depth H thus:

$$q^* = \frac{q}{(\Delta g H^3)^{1/2}}$$

This parameter plays a similar role to the fractional depth ϕ, however unlike the latter it is a function of only independent variables. Denton et al's experiments are discussed further in the ensuing sections.

4. EXPERIMENTS

4.1 Apparatus and Techniques

The experiments described here were performed in a water tunnel 3.4m long, 10cm high and 10cm wide. The tunnel was connected to a holding tank 750cm square and 700cm deep through a flexible seal. A gate separated the tunnel from the reservoir. Figure 10 gives a schematic view of the experimental apparatus. The experiment was prepared by opening the gate, tilting the tunnel down away from the holding tank and then filling the holding tank with water to a level slightly above the level of the tunnel roof. The tilt of the tunnel allowed all air to escape as it filled with water.

The gate separating the tunnel from the tank was then closed and the tunnel was brought to the horizontal position. Concentrated brine solution was added to the water in the holding tank to bring its relative density to a value between 1.01 and 1.02; the particular value was determined using a calibrated hydrometer to an accuracy of 0.0001.

The experiment was started by opening the gate to some predetermined extent thus allowing the dense brine solution to enter as a density current which displaced the fresh water originally contained in the tunnel. The progress of the density current along the tunnel was recorded photographically using a motor driven 35mm camera or alternatively a 16mm motion picture camera. Distance markers spaced at 20cm intervals along the tank enabled the velocity of the front to be evaluated to an accuracy of better than 2 per cent.

The density structure was deduced from the recorded output of conductivity probes. The probes were positioned in the centre of the tunnel at set distances above the tunnel bottom and registered horizontal conductivity profiles as the density current moved past.

Velocities were measured using the hydrogen bubble technique. The generating wire was suspended vertically across the centre of the tunnel and the motion of bubble traces leaving the wire was recorded on movie film.

Velocities were calculated from the film as described in Wilkinson (1981).

The fractional depth was controlled by adjusting the extent of the gate opening as this restricted the flow of displaced fluid from the tunnel. When the gate was fully opened a lock-exchange type flow developed in the tunnel, while partial opening of the gate reduced the value of the fractional depth.

The aim of these experiments was to determine the detailed density and velocity structure of horizontal density currents and to examine the influence of fractional depth on this structure.

4.2 Selection of the Scaling Parameters

The selection of the independent variables in miscible flows of this type is largely determined by the intended application of the experimental results. In the experiments described here the true independent variables are the effective gravitational acceleration $g' = \Delta_o g$, the height of the tunnel H and the height of the gate opening h_g. Δ_o is the relative density excess of the source. However the usefulness of a parameterisation based on say h_g/H would be very limited and will therefore not be used. In the past, the height of the following layer has usually been adopted as the relevant length scale von Karman (1940), Benjamin (1968) and Britter and Simpson (1978). However a cursory inspection of Figure 1(b) reveals that in miscible flows, the 'depth' of the following layer is not an obvious quantity and furthermore in horizontal density currents varies with distance from the head. Benjamin (1968) anticipated this difficulty and suggested that the densimetric mean level of the disturbed interface should be used in which case:

$$h = \frac{1}{\Delta o} \int_o^H \Delta dy \qquad (13)$$

where Δ is the local relative density excess.

Although this definition produces equivalent pressures at the bottom boundary it does not accurately reflect the pressure force, which is given by $\int_{oy}^{HH} \Delta\rho g \, dy \, dy$, and therefore cannot be given an exact account of the gravitational forcing. Thus in real flows, where the changes in density and velocity are continuous, the pressure and velocity fields can generally not be described in terms of a single depth parameter.

Britter and Simpson (1978) corrected for this by introducing non-dimensional coefficients whose values depended on the vertical distribution of velocity and density. The coefficients were determined from their experimental data. The resulting relationship between the normalised celerity of the front and the fractional depth became implicit and complex.

Denton et al (1981) recognised the impracticality of this form of parameterisation and instead defined the shallowness parameter $q^* = q/(\Delta g\ H^3)^{1/2}$ as the independent variable. It was an appropriate selection in their study which was concerned with intrusive flows in reservoirs where the inflow hydrograph would be a known quantity. Such is not the case in the present study where the inflow rate is a dependent variable.

It will be argued in the section dealing with density currents on gentle slopes, that in the head region, inertial forces and gravitational forces are in local equilibrium. This being the case, a length scale (ℓ) characteristic of the motion can be defined in terms of the velocity of the head (c) and the effective gravity (g′).

Thus $\ell = \frac{c^2}{g'}$

The other relevant length scale is H the total depth and the ratio $\frac{H}{\ell}$ is simply the normalised celerity of the density current which appears in (8) so that $\frac{H}{\ell} = \frac{g'H}{c^2} = F_o^{-2}$.

Scaling of the frontal structure using the characteristic length ℓ enables comparisons to be made on the effects of boundary proximity on the structure of the density front. Boundary proximity can be expressed in terms of $\frac{\ell}{H}$ or the fractional depth $\frac{h}{H}$.

5. ANALYSIS OF EXPERIMENTAL OBSERVATIONS

5.1 Distributions of Velocity and Density In Density Currents

In this section a detailed comparison is made of the internal structures of the frontal regions of density currents moving under a deep ambient layer ($\frac{H}{\ell} = 12.8$ or $F_o = 0.28$) and lock exchange flow

($\frac{H}{\ell} = 4.8$ or $F_o = 0.46$).

The term lock exchange flow in this report refers only to flow equivalent to Benjamin's energy conserving flow. Such a flow is obtained when the control weir at the entrance to the duct is completely removed permitting the displaced fluid to drain unimpeded from the duct.

The term lock exchange flow has also been used to describe any flow in which the net flow at any section is zero, irrespective of the fractional depth, (Simpson and Britter (1979) and Denton et al (1981)). In this sense all of the experiments dealing with horizontal density current would be lock exchange flows.

Figures 11(a) and 11(b) show the density structures using the same absolute scales x/H and y/H directly as they would appear to an experimental observer. Averaged isopyanals are shown for $\Delta/\Delta o$ equal to 0.9, 0.7, 0.5, 0.3 and 0.1. These contours were deduced from arrays of stationary conductivity probes which recorded the passage of the density current. The time scale was converted into a spatial scale using the transformation $t = \frac{x}{c}$ with the frontal celerity c being deduced from photographs. Instantaneous limits of salt penetration into the displaced upper flow taken from shadowgraph images are shown as the dashed lines and it is evident saline eddies penetrate well beyond what would normally be regarded as the upper boundary of the dense layer. The reasons for this are two-fold. Firstly the intensity of the shadowgraph image depends not on the absolute value of the density difference but rather on the local density gradient (or more correctly refracture index). Therefore the extremities of sheared billows produce sharp shadowgraph images while the actual density excess in the billow may be quite small. Secondly the structure of the upper shear layer is highly three dimensional and the shadowgraph boundary corresponds to the extreme position of saline material rather than some averaged position. It is evident that shadowgraphs must be interpreted with some caution.

It is interesting to compare the mean density structures in Figures 11(a) and 11(b) with the corresponding shadowgraph images shown in Figures 12(a) and 12(b) respectively. The grid lines imposed on the shadowgraphs are at vertical spacings of ℓ and horizontal spacings of 5ℓ. The homogeneous bottom layer can be clearly identified as can the stratified shear layer immediately above. The turbulent shear layer is only very weakly stratified and appears to collapse with increasing distance from the head.

The density structures shown in Figures 11(a) and 11(b) are replotted in Figures 13(a) and 13(b) respectively to scales based on the characteristic length ℓ. The vertical scale is exaggerated by a factor of 2.5 relative to the horizontal scale. It can be seen that when F_o = 0.28 (H/1 = 12.8), corresponding to a density current moving under a relatively deep ambient layer, the height of the head and the initial depth of the turbulent shear layer are appreciably greater than for a lock exchange flow when F_o = 0.46 (H/1 = 4.8). However at a distance of approximately 30ℓ behind the front the depths of the following layers are both approximately 2ℓ. It is evident from the non-uniformity of the density structure in Figures 11,12 and 13 that any definition of following layer depth is going to be rather arbitrary. Shown in Figures 14 and 15 are plots of the vertical distributions of density difference and velocity normalised with respect to the density difference of the source Δo and the celerity of the front c respectively. Figure 14 shows the distributions for the density current moving beneath a relatively deep layer (H/ℓ = 12.8). Figure 15 shows distributions within a lock exchange flow (H/ℓ = 4.8). Vertical profiles are shown at distances of x/ℓ = 5, 10, 15, 20 and 30 for the lock exchange flow and with additional profiles at x/ℓ = 40, 5 and 60 for the density flow beneath a deeper layer.

Examining first the density structures of the density flow beneath the deeper layer (Figure 14) and comparing this with the density structure shown in Figure 13(a) it can be seen that the profiles taken at x/ℓ = 5 coincides with the crest of the head of the density current. The density ratio $\Delta/\Delta o$ is less than unity over the entire depth of the flow at this section suggesting that lighter fluid is being entrained from beneath the head of the density current. This is in accord with Simpson's observations (1972). Britter and Simpson (1978) found that a strong upward flow existed at the front of the head and it is presumably this which is responsible for the uniformity of the vertical density distribution within the head. Moving back from the head into the wake region, the density distribution shows a far greater variation with depth and at x/ℓ = 10 the halocline extends over the full depth of the dense layer. Motion pictures taken of shadowgraph images revealed the presence of strong billows in the region immediately behind the head. Velocities and densities here exhibited high intermittency. The diameter of the billows was approximately 2ℓ. Moving back further behind the head, the wake generated by the billows slowly collapses as can be seen by the steepening of the density gradient with increasing x/ℓ. At distances greater than 20ℓ behind the front a layer of uniform

density can be identified beneath the stratified shear layer. The turbulent wake identified in Figure 2 lies above the stratified shear layer but because it contains no measurable density excess it does not register in the density profiles. Between $x/\ell = 10$ and $x/\ell = 30$ to 40 the depth of the stratified shear layer continues to reduce and thereafter appears to reach a stable value. The gradient Richardson number defined by:

$$Ri = g' \frac{\partial \rho}{\partial y} / \rho \left(\frac{\partial u}{\partial y} \right)^2 \qquad (14)$$

has maximum values of between 1.5 and 5 in the region of apparently stable stratified shear flow which would strongly suppress any vertical exchange.

The density structure of the lock exchange flow ($H/\ell = 4.8$) shown in Figure 15 has a similar general character to the density flow beneath a deeper layer just described. However there are important differences in detail. The depth of the homogeneous layer at the bottom of the density current is appreciably deeper for the lock exchange flow suggesting that energy available for mixing is also less. This is in agreement with Benjamin's model for density currents where he showed that the rate of energy dissipation relative to the total energy flux reduced as the fractional depth became smaller. Density gradients within the stratified shear layer are steeper for the lock exchange flow.

Vertical distributions of the horizontal velocity component are also shown in Figures 14 and 15 at the same sections as the previously described density profiles. It is apparent at the moderate Reynold's numbers of these experiments (typically 4,000 for the lock exchange experiments and 2,000 for the deep ambient layer experiments based on the height and celerity of the head) that boundary layer development has an appreciable influence on the velocity structure. The effects of friction on the flow are not insignificant. Outside the boundary layer velocities correspond closely with the density structure. Velocity maxima occur near the top of the homogeneous layer and in the absence of boundary friction flow within this layer would be uniform. Strong shear is evident through the halocline and close to the head the flow in this region was turbulent. Mixing associated with this turbulence can be clearly seen in the shadowgraphs in Figure 12. Further downstream from the head turbulence in the halocline is suppressed and the flow becomes laminar.

The thickness of the stratified shear layer relative to the depth of the underlying homogeneous layer tends to increase as the fractional depth becomes smaller.

5.2 Stability of the Shear Layer

It can be seen from a cursory inspection of the shadowgraphs in Figures 12(a) and 12(b) that the intensity of interfacial disturbance decreases with distance from the head. The stability of stratified shear flow may be expressed in terms of the gradient Richardson number introduced previously. In this section Ri is based on the density and velocity gradients at the inflexion point of the vertical density distribution. Thus the values given for Ri are maximum values within the halocline. It is generally accepted that if Ri is less than about 1/4 the destabilising effect of shear will over-ride the stabilising influence of gravity and turbulent mixing will result. On the other hand if Ri exceeds 1/4 gravity will tend to suppress any turbulence and ultimately the flow will become laminar.

The gradient Richardson number of the stratified shear layer is plotted as a function of the normalised distance from the head in Figure 16 for the lock exchange flow. The stratified shear layer in this flow did not exhibit the periodic irregularities caused by the presence of billows which were very apparent for experiments with smaller fractional depths. Strong mixing was evident for a distance of about 15ℓ behind the head in the lock exchange flow. (See Figure 12(b)). Over the same range in Figure 16 it can be seen that the gradient Richardson numbers are less than the critical value of 1/4. Beyond $x/\ell = 15$ there is obvious suppression of turbulence and a steepening of the halocline. Ri values tend to stabilise towards the value 0.35 ± 0.1 obtained by Britter and Simpson (1978) in their experiments with stationary fronts. (See also the density profiles in Figure 15). Gradient Richardson numbers in this region are greater than the critical value and the shear is insufficient to maintain turbulent exchange across the halocline.

5.3 Volume and Density Fluxes

The normalised fluxes of volume and density excess beneath the level of flow reversal are plotted against the non-dimensional distance parameter (x/ℓ) in Figures 17 and 18 respectively. Fluxes are shown for $H/\ell = 12.8$

and 4.8 in each of these figures. In the frontal region (x/ℓ = 0 to 30) the fluxes of volume and density excess have values of (2.3 ± 0.2) and (2.0 ± 0.4) $c\ell$ and (1.5 ± 0.2) and (1.7 ± 0.2)$\Delta oc\ell$ for the deep ambient layer and lock exchange experiments respectively. It will be noted that although the normalised volume flux is greater for the density current flowing beneath a deep ambient layer the flux of density difference is less. This is due to the relatively deeper homogeneous layer in the lock exchange flow.

Because of friction the velocity distribution is non-uniform so that an observer moving with the front would see a circulation from the homogeneous layer into the stratified shear layer above and into bottom boundary layer below. Simpson and Britter (1979) defined a parameter quantifying this circulation as $g'q_c/C^3$ where q_c was the circulating flow. In their steady state experiments q_c was the make-up flow while in their unsteady experiments q_c was estimated by tracking dye traces. When plotted against their fractional depth h_4/H both methods gave similar values of $g'q_c/C^3$ ranging from 0.13 for $h_4/H \sim 0.1$ to 0.25 for lock exchange flows.

In the present series of experiments q_c was obtained from the velocity profiles which were integrated between the two levels where u = c i.e.

$$q_c = \int_{y_u=c}^{y_u=c} (u-c)dy$$

The circulation parameter defined by Simpson and Britter (1979) can also be expressed in terms of the characteristic length (ℓ) by substituting $g'/c^2 = 1/\ell$ to give

$$\frac{g'q_c}{c^3} = \frac{q_c}{c\ell}$$

For the lock exchange flow (Fo = 0.46 and h_4/H = 0.24) the circulation parameter was found to have a value of 0.18 ± 0.10 while for the density current under a relatively deep layer (Fo = 0.28 and $\frac{h_4}{H}$ = 0.10) the circulation parameter was found to be 0.12 ± 0.06. Both figures are in agreement with those obtained by Simpson and Britter (1979).

The values of the circulation parameter were taken at six equally spaced sections between the head and $x/\ell = 30$. No systematic variation with distance from the head was detected although the large variance associated with the calculation of the circulation could well have masked any variation with x. The large variance was due to the small differences between u and c.

The level at which the horizontal velocity component reverses sign ($y_u = 0$) normalised with respect to ℓ is plotted against the normalised distance from the head in Figure 19 for the two flows in Figures 17 and 18. Because of the relatively deeper mixed layer at smaller values of the fractional depth the level of flow reversal is more elevated than is the case for a lock exchange flow.

5.4 Defining a Layer Depth

In real density currents, friction causes the pycnoclines to be inclined to the horizontal. This effect is clearly visible in Figure 13 where pycnoclines are plotted to show the density structure of the frontal region of a density current. It is therefore evident that any definition of the following layer depth must be rather arbitrary because of the non-uniformity of the layer. In order to examine this more closely, Benjamin's recommendation that the densimetric mean level of the disturbed interface is adopted as representative of the layer depth. This depth h was defined in Equation 13 and is plotted non-dimensionally against distance from the head in Figure 20 for the two flows previously described. It is worth noting that there is no significant difference between the normalised depths of the two layer at distances greater than about 20ℓ from the front. It would appear that the density structure of the flow is only Froude number dependent in the immediate vicinity of the head where frictional forces are not yet dominant.

The increasing values of h with increasing distance from the front is a result of boundary friction. For a density current moving travelling along a horizontal surface beneath a deep overlying layer, the force balance some distance behind the head, is dominated by gravity and friction. Inertial effects are relatively small and in a first approximation may be neglected. An estimation is now made of the distance from the front at which the total frictional force is comparable with horizontal pressure force acting at the front of the density current.

The force balance proposed above implies that:

$$\frac{\partial p}{\partial x} + \frac{\partial \tau}{\partial y} = 0$$

within the flowing layer. Integration over a control volume extending from a section (0) of reasonably parallel flow just behind the head to a section (1) further behind the head gives:

$$\int_{x_o}^{x_1} \tau_b dx = \int_{o}^{H} p dy$$

where τ_b is the boundary shear stress. If a simple two layer system is assumed then

$$\tau_b dx = \rho g' \left[h_{x1}^2 - h_{xo}^2\right]$$

At the section where

$$\int_{x_o}^{x_1} \tau_b dx = \Delta\rho g' h_{xo}^2/2$$

Substitution for the friction force term in (14) gives

$$h_{x1} = \sqrt{2}\, h_{x0}$$

Figure 20 shows that just behind the head $h_{x0} \sim 1.7\ell$ so that frictional effects can be regarded as dominant when $h_{x1} \sim 2.4\ell$. For the experiment with a deep ambient layer $h_{x1} \sim 2.4\ell$ when $x/\ell \sim 80$. Thus frictional effects can only be considered negligible (say less than 10% of $\rho g' h_{xo}^2/2$) for distances of the order of 10ℓ from the head and beyond this frictional influence become increasingly important component of the force balance. Therefore for the purposes of defining a fractional depth the height of the mean piezometric level above the bottom boundary h at a distance of 15ℓ from the front is chosen. This follows Benjamin's original definition of the fractional depth in miscible density flows.

Other investigators have used a variety of definitions for the depth of the following layer. Middleton (1966), Barr (1967) and Wilkinson and Wood (1972) dyed the dense layer so as to identify its depth (h_{vis}).

It was found during the course of these experiments that the use of dye to define the depth of the following layer produced inconsistent results unless the dye concentration and in particular the lighting were carefully controlled. For this reason dye is not recommended as a means of defining depths in stratified flows where interfacial mixed may occur.

Britter and Simpson (1978) used shadowgraph technique from which the depth of the homogeneous layer (h_4 in Figure 8) could be readily observed).

The various length scales are compared for the deep ambient layer (H/ℓ = 12.8, Fo = 0.28) and the lock exchange flow (H/ℓ = 4.8, Fo = 0.46) at a distance of 15ℓ from the front in Table 1.

TABLE 1

	F_o = 0.28	F_o = 0.46
h/H	0.128	0.35
$\ell/h = \frac{c^2}{g'h}$	0.63	0.59
h_{vis}/h	1.5	1.4
h_4/h	0.78	0.68

Note: h_{vis} is sensitive to the dye concentration and lighting.

It can be seen from Table 1 that the ratio ℓ/h and h_{vis}/h are relatively insensitive to the fractional depth h/H. Recalling that $\ell/h = \frac{c^2}{g'h}$ its value is seen to increase with reducing values of the fractional depth as predicted by Benjamin's original model. The ratio h_{vis}/h also increases slightly with reducing F_o indicating the presence of a relatively deeper shear layer when the overlying layer is deep.

At first sight the increase in the relative depth of the homogeneous layer h_4/h is surprising however this is required to achieve the higher values of the normalised celerity F at smaller fractional depths. Britter and Simpson's criticism of the quantitative accuracy of Benjamin's theory when their comparisons were based on a layer depth defined by h_4, would appear to be unjustified. Much closer agreement with Benjamin's theory would have been obtained had Benjamin's original definition of layer depth

h been adopted. The experiments of Wilkinson (1982) showed that the Benjamin model accurately predicted the behaviour of steady immiscible frontal flows.

5.5 Celerity of the Front

Successive models of the relationship between the celerity of a density current front and the depth of the following layer have produced increasingly realistic models with a corresponding increase in the degree of parameterisation.

Von Karman's original model assumed that the flow was energy conserving and that the overlying layer was very deep. Benjamin made the next significant contribution by examining the fundamental balance of forces and demonstrated the effect of limited depth in the overlying layer. Yih (1963) had previously recognised the differences the normalised celerities of a lock exchange flow and a density current moving beneath a deep layer. Britter and Simpson incorporated a homogeneous bottom layer overlain by a stratified shear layer into their model and showed that circulation at the head between these layers had an appreciable influence on the celerity of the front at values of the fractional depth of less than 0.1.

Experimental values of the normalised celerity $c/(gh)^{1/2}$ are plotted against the fractional depth $\frac{h}{H}$ in Figure 21. The plotted curve corresponds to Benjamin's relationship between the same variables in a two layered flow. The comparison is favourable for values of the fractional depth of greater than 0.15. The fractional depth in the case of the lock exchange flow was 0.35 compared with 0.50 for an immiscible exchange flow (Wilkinson, 1982). However, the value of the normalised celerity (0.77) compares reasonably with Benjamin's value for a two layer system of $1/\sqrt{2}$ (= 0.707).

It is of interest to examine the effect elevation of the nose or leading edge of the density current has on its celerity. Benjamin (1968) demonstrated that if the forward stagnation point is elevated above the boundary the celerity of the density current is reduced. Wilkinson (1982) revised Benjamin's calculations making allowance for elevation of the stagnation point and for the effects of surface tension. (Surface tension effects proved to be significant for air cavities but are not important in the present study). Wilkinson's analysis introduced another parameter h_5 the height of the nose into the analysis (see Figure 8).

Simpson (1972) found that the elevation of the nose of a density current relative to the maximum height of the head h_0 could be expressed as a function of a Reynold's number based on the celerity of the head and its height. This relationship was shown to be:

$$\frac{h_s}{h_o} = 0.61 \quad (ch_o/\upsilon)^{-0.21} \tag{15}$$

By means of a correct transformation Wilkinson (1982) showed that the stagnation point did not occur at the nose but at approximately half the nose height from the boundary. The presence of a boundary layer in the displaced fluid ahead of the front tends to move the stagnation point closer to the nose.

The dashed curve in Figure 21 shows a modified version of Benjamin's equation for the celerity of the front after allowance was made for the elevation of the stagnation point as described by Wilkinson (1982). Simpson's relationship (Equation 15) was used to estimate the height of the nose.

This corrected relationship for the normalised celerity of the front is plotted in Figure 21 and shows the same tend as the experimental data for fractional depths greater than 0.09. The systematic deviation for Benjamin's idealised two layer relationship can therefore be accounted for by the elevation of the nose of the density current above the boundary. The fact that the corrected curve also agrees numerically with the experimental data is largely fortuitous as the dashed curve is still based on a simple two layered model.

The single data point which departs significantly from the other data ($h/H = 0.057$) and a Reynold's number of 480 (based on the celerity and height of the head). It is probable that this departure is due to other frictional effects because apart from the region immediately behind the head the flow in this experiment was laminar.

5.6 A Note on Fractional Depths in the Range $0.5 > h/H > 0.347$

The maximum fractional depth obtained in the experiments was 0.35 and was observed in the lock exchange flows. It can be easily shown that the flow in the displaced layer (the upper layer in these experiments) was internally supercritical for fractional depths between 1/2 and 0.347. Benjamin (1968) argued that in these cases a hydraulic jump would occur forcing the displaced layer to its conjugate subcritical state. This can be seen more clearly in Figure 22 where the data from the previous figure is replotted in terms of the total depth H.

It is evident that the supercritical flow state is not realised as originally surmised by Benjamin.

5.7 Nature of the Wake and Height of the Head

It was shown in Section 2 that in order to achieve a balance between pressure forces and momentum a density current front must occur on energy loss. The wake which develops in the lee of the head provides the mechanism by which the energy excess is dissipated. Inspection of the shadowgraphs in Figure 12 gives the impression that the thickness of the wake reduces with distance from the head. This conclusion is erroneous and is due to the fact that the shadowgraph only registers the presence of salinity gradients and does not indicate the presence of low level turbulence.

The extent of the wake was measured by observing the distortion of a vertical dye trace in the displaced layer as the density current flowed beneath it. The dye trace was obtained by dropping small crystals of potassium permanganate through an open stand pipe in roof of the duct prior to commencement of the dense inflow. The trace left by the crystal as it fell through the duct was filmed during the passage density flows and turbulent and non-turbulent regions could be readily identified. The height of the turbulent region (the wake) above the head of the front normalised with respect to the characteristic length ℓ is plotted against the normalised distance from the head $x-x_0/\ell$ in Figure 23. The relevant variables are also defined in the figure. Data are shown for the wake spread for density currents with relative depths H/ℓ of 5.0, 6.6 and 8.2. It is clear that the spread is similar in all cases and the height of the wake varied as the half power of the distance from the head until its growth was limited by the upper boundary. The power relationship for the wake is the

same as that behind any bluff body in homogeneous flow (Goldstein, 1938). Turbulence intensities behind the head are insufficient to produce dispersion of the dense fluid over the full depth of the wake. Instead the dense fluid is confined to a stratified shear layer at the bottom of the wake and this tends to collapse with distance from the head as was seen in the shadowgraphs in Figure 12.

6. FORM DRAG OF THE HEAD OF A DENSITY CURRENT.

A drag coefficient for the head of a density current based on the height and celerity of the head can be evaluated by equating the rate of energy dissipation associated with motion of the head to the rate of work done against the drag force exerted by the flow on the head. The characteristics of the flow associated with the head can be evaluated using the conservation relationships for volume, mass and momentum. The distributions of density excess and velocity are based on those observed by Simpson and Britter (1979) in their experiments.

The schematisation of the gravity current head, and variable definitions adopted by Simpson and Britter are used here and are reproduced in figure 8. Steady motion is obtained by moving with the head at velocity c. The calculations are performed over a control volume which extends sufficiently far either side of the head for the flow to be assumed uniform. It is assumed that at section BB behind the front, the flow consists of a homogeneous layer with velocity u_4 and density excess $\Delta_4\rho$. Above this lies a stratified shear layer of thickness h_3 where the velocity changes from $-u_4$ to U and the density excess from $\Delta_4\rho$ to zero. Simpson and Britter found from their experiments that the variation of density excess and velocity across the shear layer could be described by the relationships

$$\Delta = \Delta_4 \left(\frac{h}{h_3} \right)^4 \qquad (16)$$

and

$$u = U \left[1 - \left(1 - \frac{u_4}{U} \right) \left(\frac{h}{h_3} \right)^4 \right] \qquad (17)$$

where h is measured vertically downwards from the level of the crest of the gravity current head.

The total depth parameter $H^* = H/h_4$ is taken as the independent variable and determines the thickness of the shear layer $h_3^* = h_3/h_4$ and the velocity of the front which can be characterised by a Richardson number defined as

$$Ri = \frac{\Delta_4 \, g h_4}{c^2} \qquad (18)$$

It remains then to calculate the following non-dimensional variables: the elevation of the free surface $\eta^* = \eta/h_4$, the velocity of the upper layer $U^* = U/c$ and the velocity of the lower layer $u_4^* = u_4/c$ by simultaneous solution of the three conservation relationships.

Continuity of volume flux at sections upstream and downstream of the front in figure 8 requires that

$$cH = \int_0^{H+\eta} u \, dz \qquad (19)$$

which to order Δ (or η/H) can be expressed as

$$U^* = \frac{5H^* + u_4^* (5 + h_3^*)}{5H^* - h_3^* - 5} \qquad (20)$$

after u has been expressed in terms of h/h_3 within the shear layer using (17).

Continuity of the flux of density excess across the control volume requires that:

$$\int_o^H \Delta \, u \, dz = 0 \qquad (21)$$

and again after substitution for Δ and u in terms of h/h_3 within the shear layer (21) reduces to:

$$u_4^* = \frac{4 U^* h_3^*}{45 + 5h_3^*} \qquad (22)$$

Finally conservation of flow force across the control volume requires that to order Δ,

$$\rho c^2 H + \frac{\rho g H^2}{2} = \int_o^{H+\eta} (p + \rho u^2) \, dz$$

which after substitution for Δ and u using 16 and 17 gives

$$\eta^* = \frac{1}{Ri\ H^*}\left[H_* - U^{*2}\,(H^* - h_3^* - 1) - u_4^{*2} + \left(1 - \frac{2\alpha}{5} + \frac{\alpha^2}{9}\right) U^{*2}\, h_3^* + Ri\left(\frac{h_3^{*2}}{30} + \frac{h_3^*}{5} + \frac{1}{2}\right)\right] \qquad (23)$$

where

$$\alpha = 1 - u_4^*/U^* \qquad (24)$$

The conservation equations (20), (22) and (23) can be solved explicitly for U^*, u_4^* and η^* in terms of the independent variable H^*. The layer Richardson number Ri and the thickness of the shear layer h_3^* are obtained from Simpson and Britters' experiments.

The drag coefficient C_D can now be obtained by equating the rate of energy dissipation by the drag force acting on the head of the gravity current to the change in the energy flux across the control volume. Thus

$$C_D\,(h_3 + h_4)\,\rho c^3 = \left(\frac{c^2}{2} + gH\right)\rho cH - \int_o^{H+\eta}\left[\rho\,\frac{u^2}{2} + p + \rho(1 + \Delta)gz\right]u\,dz \qquad (25)$$

When substitutions are made for the density and velocity distributions across the shear layer the following results

$$C_D = \frac{P_k + P_p}{h_3^* + 1} \qquad (26)$$

the change in the normalised flux of kinetic energy P_1 is given by

$$P_k = \frac{1}{2} \{ H^* + u_4^{*3} - U^{*3} [H^* - h_3^* (\frac{3\alpha}{5} - \frac{\alpha^2}{3} + \frac{\alpha^3}{13}) - 1] \} \qquad (27)$$

and the change in the normalised flux of pressure and elevation energy P_2 is given by

$$P_p = Ri \{U^* h_3^{*2} (\frac{7\alpha}{225} - \frac{1}{15}) + h_3^* [U^* (\frac{\alpha}{9} - \frac{1}{5}) + \frac{u_4^*}{5} + \frac{h_3^*}{30} + \frac{1}{5}] + u_4^* + \frac{1}{2} \} +$$

$$+ H^* - U^{*2} (H - h_3 - 1) - u_4^{*2} + (1 - \frac{2\alpha}{5} + \frac{\alpha^2}{9}) U^{*2} h_3^* \qquad (B-13)$$

In the table below, h_3^* and Ri were obtained for the different values of the independent variable H* using Simpson and Britters' experimental results, u_4^* was calculated using (20) and (22) and finally C_d evaluated using (23), (24) and (26).

H*	h_3^*	Ri	u_4^*	C_d
20	2.7	0.64	0.20	0.205
10	2.0	0.74	0.17	0.211
6.7	1.4	1.00	0.14	0.271
5	1.1	1.23	0.12	0.314

7. REFERENCES

[1] Barr, D.I.H. "Densimetric exchange flow in rectangular channels, Part III", La Houille Blanche, 12 , 1967, pp 619-632.

[2] Barr, D.I.H. "Density currents and public health engineering", Water and Water Engineering, 70 , No. 850 1966, pp 508-514.

[3] Benjamin, T.B. "Gravity currents and related phenomena", J. Fluid Mechanics, 31 , Part 2, 1968, pp 209-248.

[4] Britter, R.E. and Linden, P.F. "The motion of the front of a gravity current travelling down an incline", J. Fluid Mechanics, 99 , 1980, pp 531-543.

[5] Britter, R.E. and Simpson, J.E. "Experiments on the dynamics of a gravity current head", J. Fluid Mechanics, 88 , 1978, pp 223-240.

[6] Denton, R.A., Fanst, K.M. and Plate, E.J. "Aspects of stratified flow in man-made reservoirs", Inst. Wasserbau III, Univ. Karlsruhe, Report 20, 1981.

[7] Goldstein S. "Modern developments in fluid dynamics", Vol. I, Dover, 1964.

[8] Harris, G.S. "An inclined plume", A.S.C.E. Proc. Engineering Mechanics Div. E.M.1., Feb, 1965 pp 7-18

[9] Hebbert, B., Imberger, J., Loh, I. and Patterson, J. "Collie river underflow into the Wellington reservoir", A.S.C.E., J. of the Hydraulics Div. HYS, May, 1979, pp 533-546.

[10] Hopfinger, E.J. and Tochon-Dangay J.C., "A model study of powder-snow avalanches", Glaciology 19 , (81), 1977, pp 343-356.

[11] Karman, T.H. von., "The engineer grapples with non-linear problems", Bull. Amer. Math. Soc. 46 , 1940, pp 615-683.

[12] Keulegan, G.H. "Thirteenth progress report on model laws for density currents", U.S. Natl. Bur. Standards Report 5186, 1957.

[13] Keulegan, G.H. "Twelfth progress report on model laws for density currents", U.S. Natl. Bur. Standards Report 5831, 1958.

[14] Keunen, Ph.H. "Estimated size of the grand banks turbidity current", American J. of Science, 250 , Dec, 1952, pp. 874-884.

[15] Middleton, G.V., "Experiments on density and turbidity currents II: uniform flow of density currents", Canadian J. of Earth Sciences, 3 , Oct. 1966, pp 627-637.

[16] Simpson, J.E. "Effects of the lower boundary on the head of a gravity current", J. Fluid Mechanics, 53 , 1972, pp 759-768.

[17] Simpson, J.E. "Sea breeze fronts", Quart. J. Royal Meteorological Soc. 95 , 1969, pp 758-761.

[18] Simpson, J.E. and Britter, R.E. "The dynamics of the head of a gravity current advancing over a horizontal surface", J. Fluid Mechanics, 94 , 1979, pp 477-495.

[19] Wilkinson, D.L. "Motion of air cavities in long horizontal ducts", J. Fluid Mechanics (1982), 118 , pp 109-122.

[20] Wilkinson, D.L. "Studies in density stratified flow", Univ. of New South Wales Water Research Laboratory Report No. 118, April, 1970.

[21] Wilkinson, D.L. and Willoughby, M.A. "Velocity measurement with hydrogen bubbles - the wake correction", J. of Hydraulic Research, 19, 1981, No. 2, pp 141-153.

[22] Wilkinson, D.L. and Wood, I.R. "Some observations on the motion of the head of a density current", J. Hydraulic Research 10, 1972, No. 3, pp 305-324.

[23] Wood, I.R. "Studies in unsteady self preserving turbulent flows", Univ. of New South Wales Water Research Laboratory Report No. 81, 1965.

[24] Yih, C.S. "A study of the characteristics of gravity waves at an interface", M.S. thesis, State University of Iowa, 1947, (see Yih (1965)).

[25] Yih, C.S. "Dynamics of non-homogeneous fluids", MacMillan, 1965.

LIST OF FIGURES

12a Shadowgraph of a density current with F = 0.28

12b Shadowgraph of a density current with F = 0.46

13a Density structure in terms of y/ℓ and x/ℓ for $F_o = 0.28$

13b Density structure in terms of y/ℓ and x/ℓ for $F_o = 0.46$

14 Non-dimensional distributions of density difference and velocity at various vertical sections in density current travelling beneath a deep layer ($H/\ell = 12.8$).

15 Non-dimensional distributions of density difference and velocity at various vertical sections in lock exchange flow ($H/\ell = 4.8$).

16 Gradient Richardson number of the stratified shear layer as a function of normalised distance from the head in a lock exchange experiment.

17 Normalised volume flux as a function of distance from the head.

18 Normalised flux of density excess as a function of distance from the head.

19 Level of velocity reversal as a function of distance from the front.

20 Hydraulic mean level of the interface as a function of normalised distance from the head.

21 Froude number of a density current front as a function of the fractional depth.

22 Normalised celerity of a density current front as a function of the fractional depth.

23 Growth of the wake as a function of distance from the head of a density current.

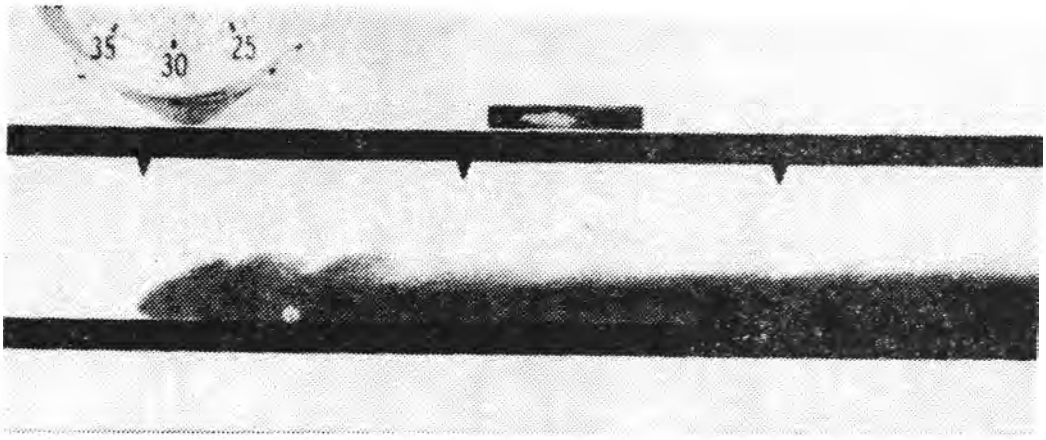

FIGURE 1a. THE FRONTAL REGION OF A DENSITY CURRENT IN WHICH THE DENSER LAYER HAS BEEN DYED. F_o=0.35.

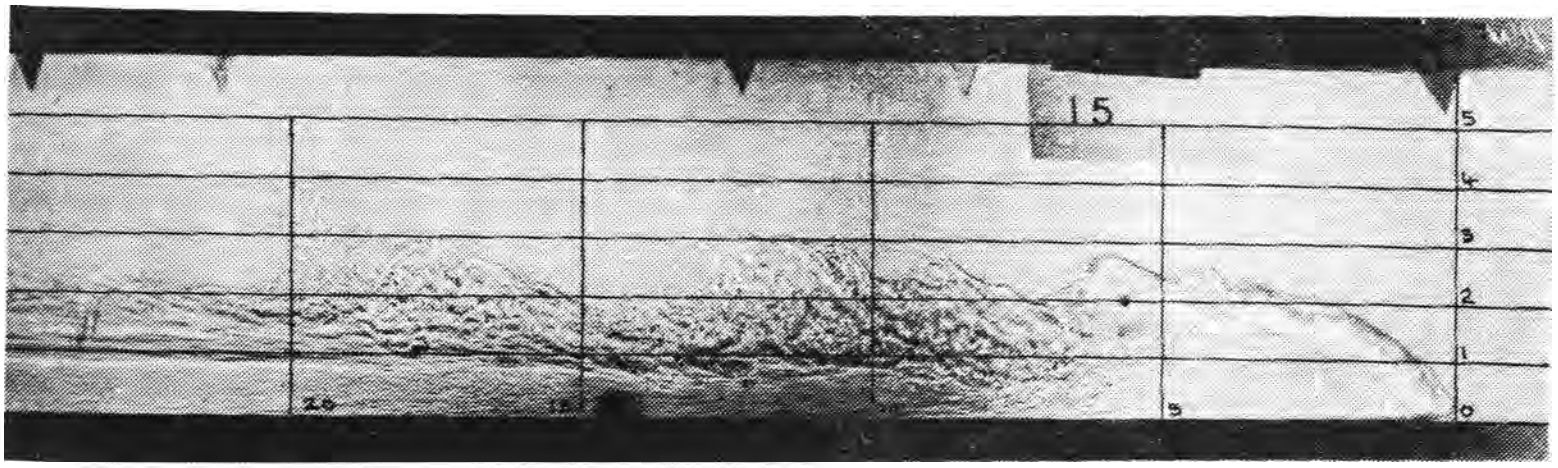

FIGURE 1b: A SHADOWGRAPH IMAGE OF A DENSITY CURRENT FRONT THE SAME AS THAT SHOWN IN FIGURE 1A. THIS TECHNIQUE ENABLES THE VARIOUS REGIONS WITHIN THE DENSITY CURRENT TO BE IDENTIFIED.

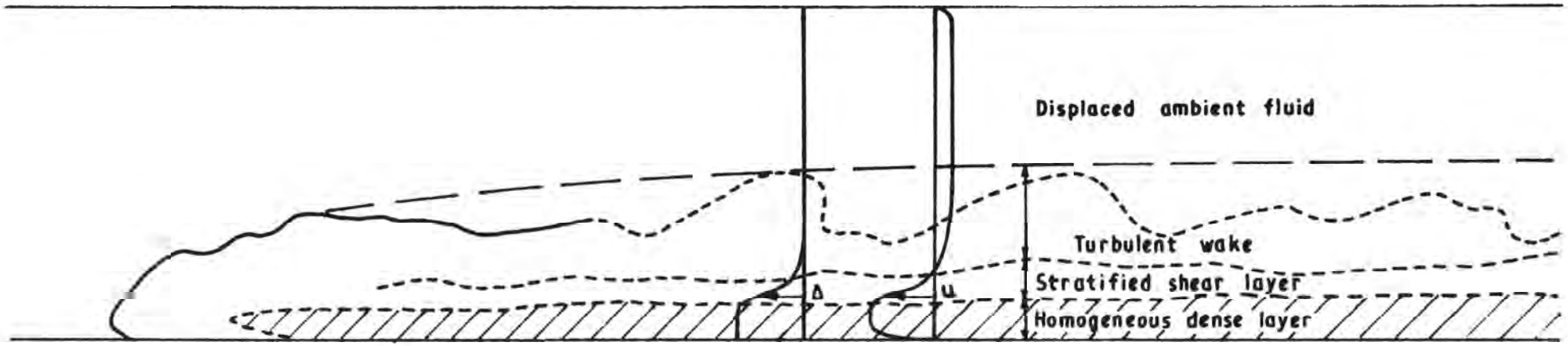

FIGURE 2: SKETCH OF A DENSITY CURRENT IN WHICH THE DIFFERENT REGIONS ARE IDENTIFIED.

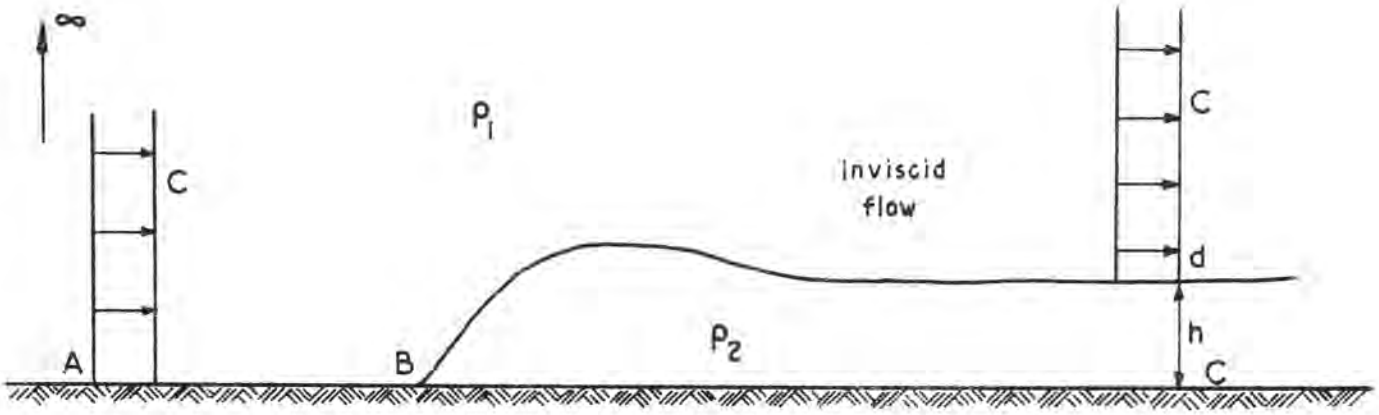

FIGURE 3: VON KARMAN'S IDEALISED MODEL OF THE HEAD OF A DENSITY CURRENT

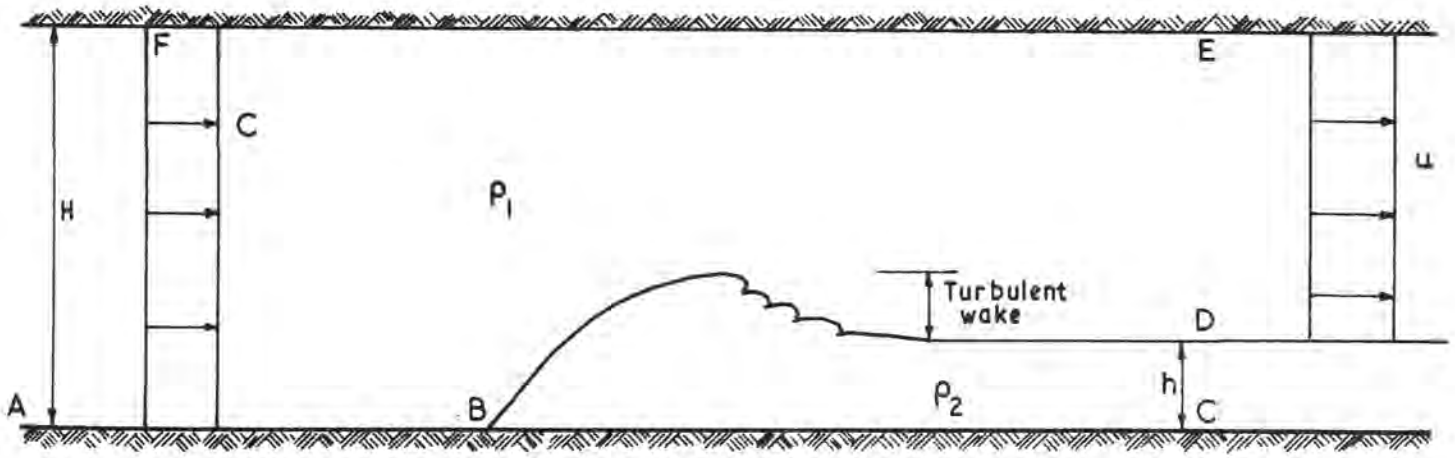

FIGURE 4: BENJAMIN'S CONCEPTION OF THE FRONTAL REGION OF A DENSITY CURRENT

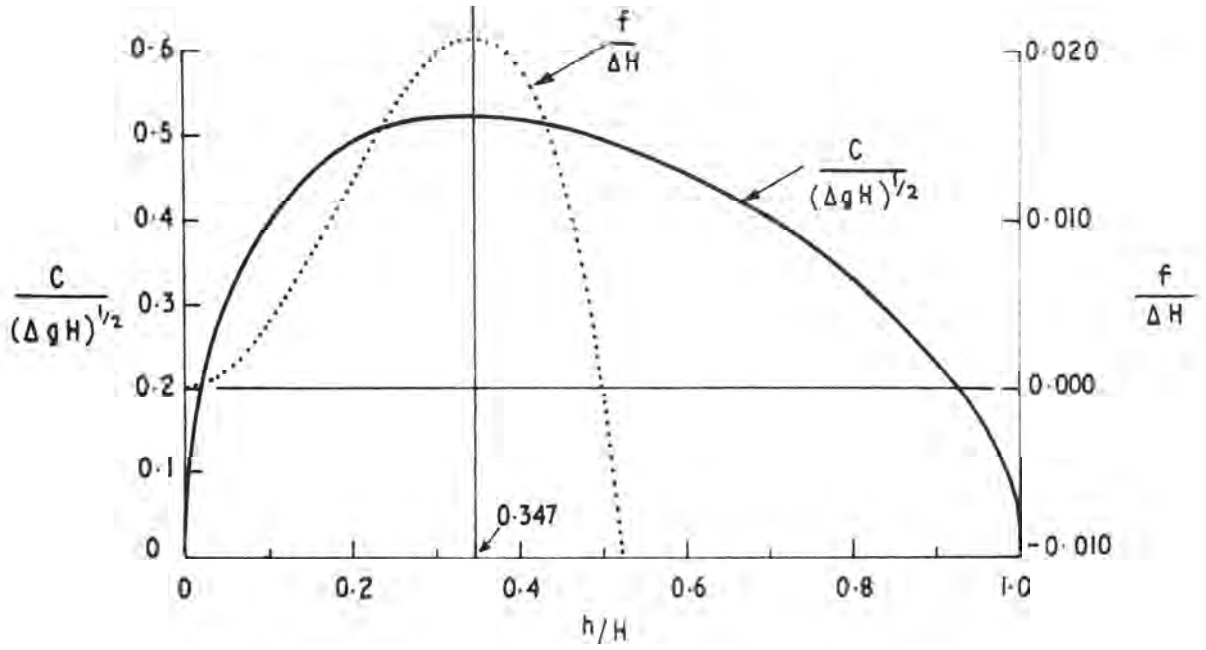

FIGURE 5: CELERITY OF AND HEAD LOSS ACROSS THE HEAD OF A DENSITY CURRENT NORMALISED WITH RESPECT TO THE DISTANCE BETWEEN CONFINING BOUNDARIES AS A FUNCTION OF THE FRACTIONAL DEPTH.

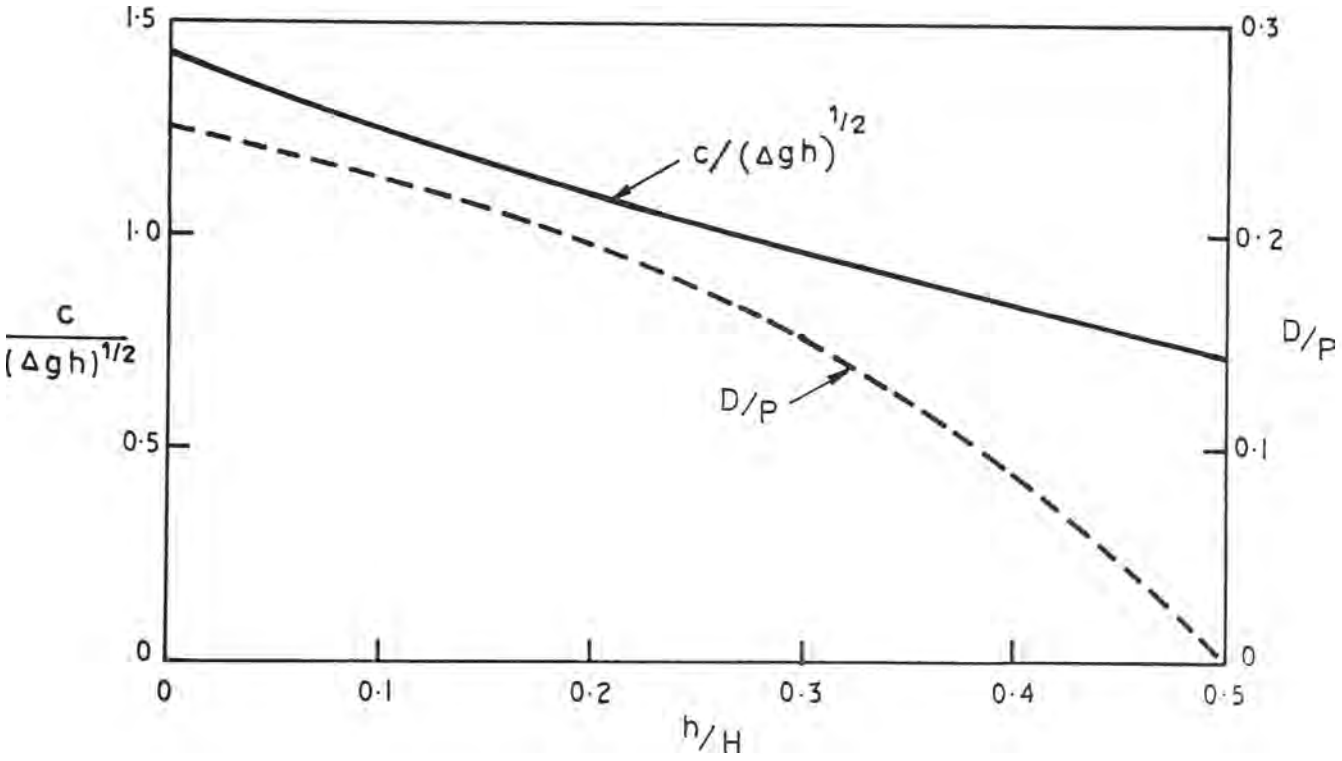

FIGURE 6: CELERITY AND RATE OF ENERGY DISSIPATION AT THE HEAD OF A DENSITY CURRENT NORMALISED WITH RESPECT TO THE DEPTH AND ENERGY FLUX OF THE FOLLOWING LAYER AS A FUNCTION OF THE FRACTIONAL DEPTH.

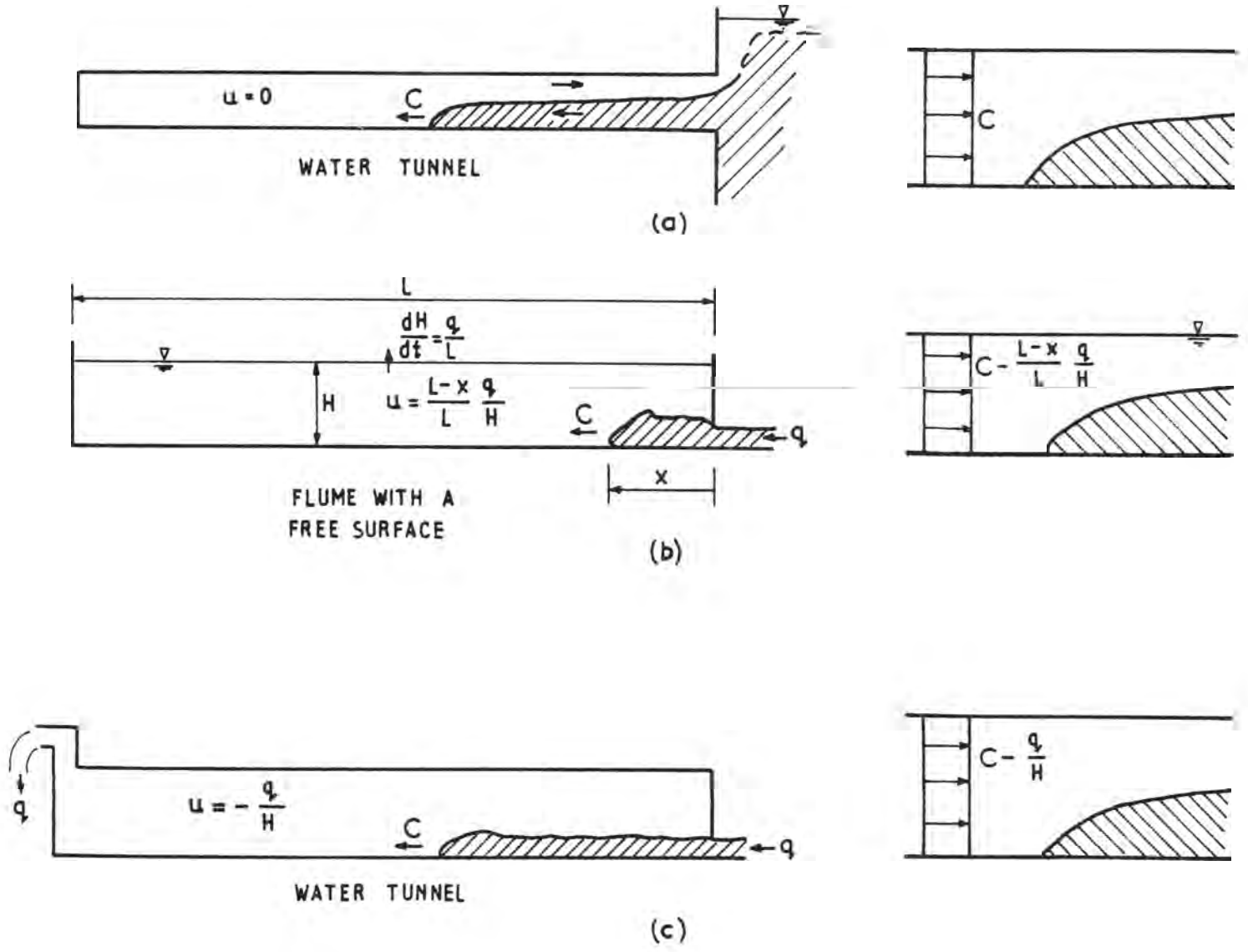

FIGURE 7: EFFECT OF AND CONDITIONS ON THE MOTION OF A DENSITY CURRENT.

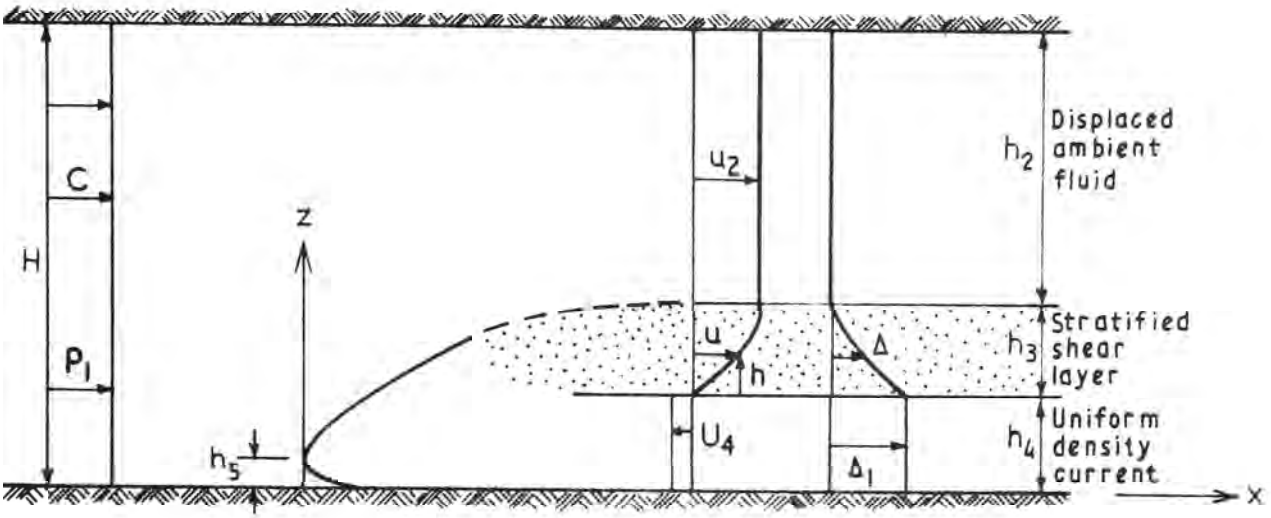

FIGURE 8: BRITTER AND SIMPSON'S SCHEMATISATION OF THE FRONTAL REGION OF A DENSITY CURRENT

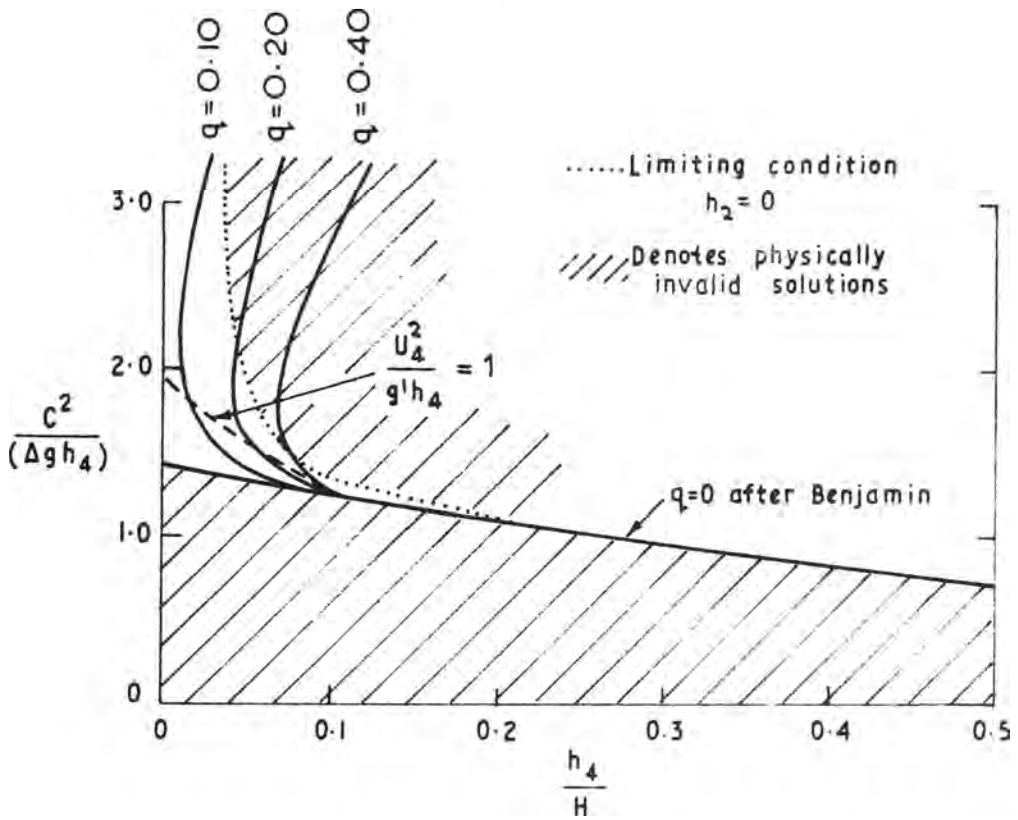

FIGURE 9: FROUDE NUMBER OF A DENSITY CURRENT FRONT AS A FUNCTION OF THE FRACTIONAL DEPTH AND THE CIRCULATION PARAMETER.

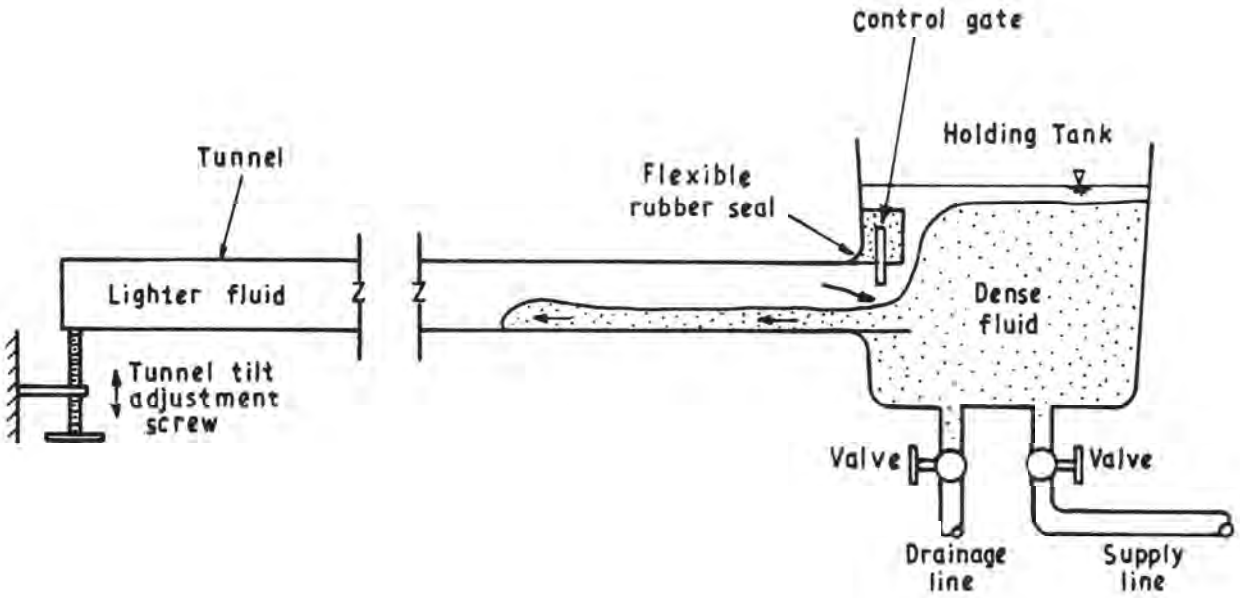

FIGURE 10: SCHEMATIC VIEW OF THE WATER TUNNEL

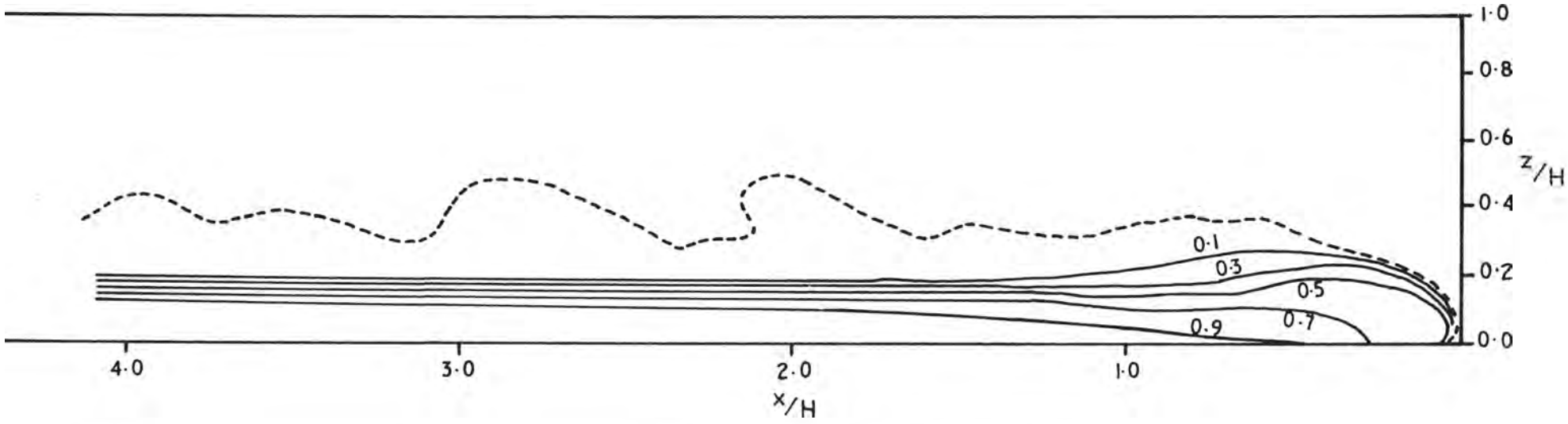

FIGURE 11a:DENSITY STRUCTURE FOR IN TERMS OF y/H AND x/H FOR F_0 = 0.28

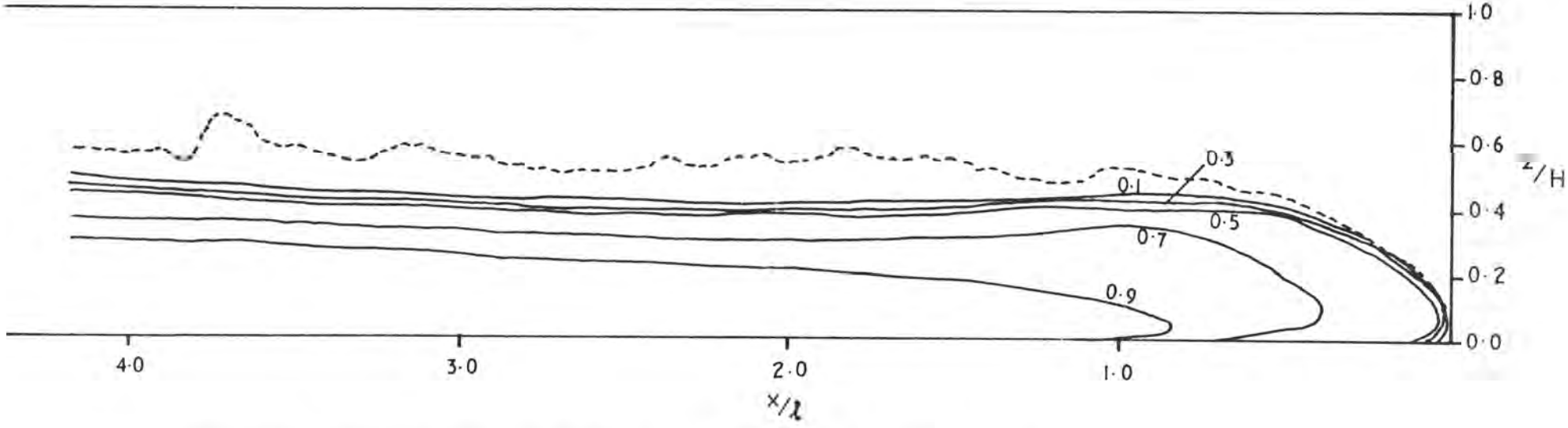

FIGURE 11b:DENSITY STRUCTURE FOR IN TERMS OF y/H AND x/H FOR F_0 = 0.46

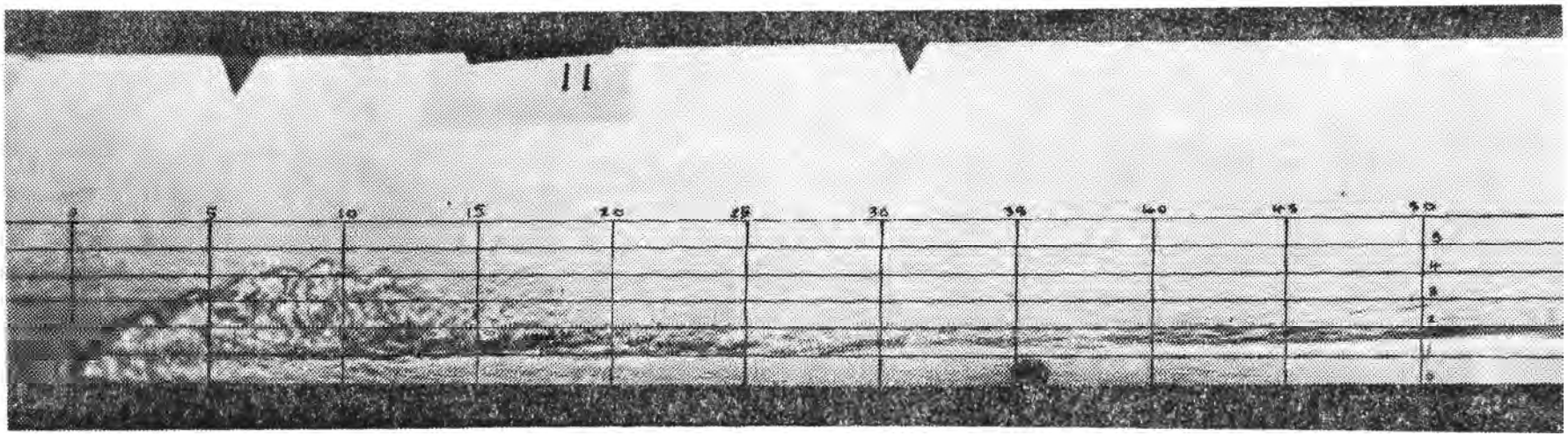

FIGURE 12a : SHADOWGRAPH OF A DENSITY CURRENT FRONT FOR F_o = o.28. THE GRID LINES ARE NORMALISED.

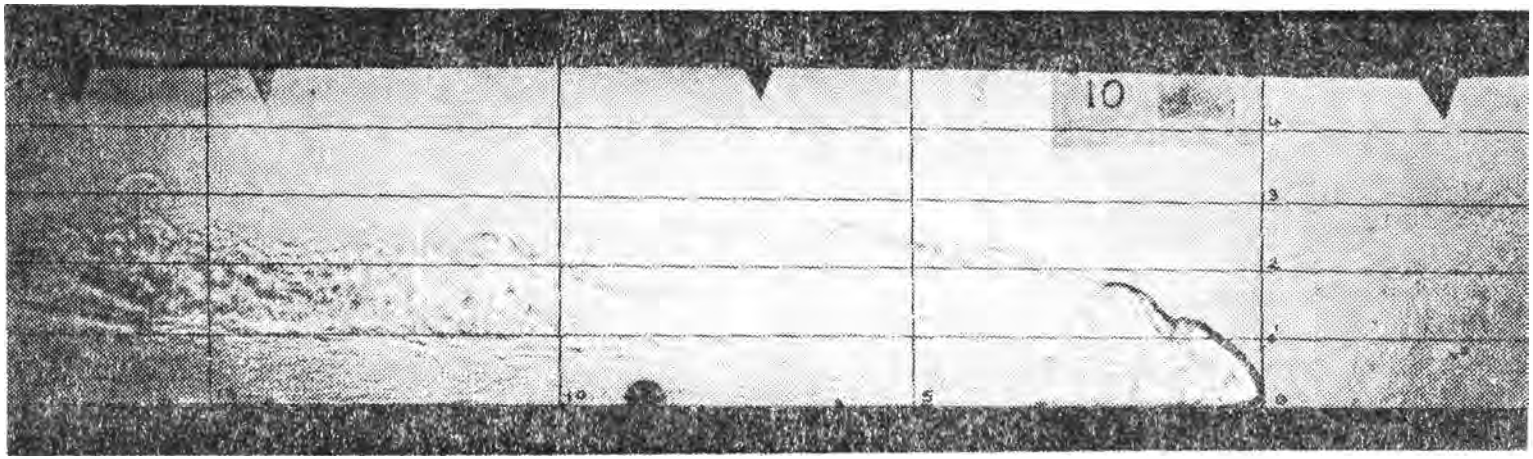

FIGURE 12b : SHADOWGRAPH OF A DENSITY CURRENT FRONT FOR F_o = 0.46. THE GRID LINES ARE NORMALISED.

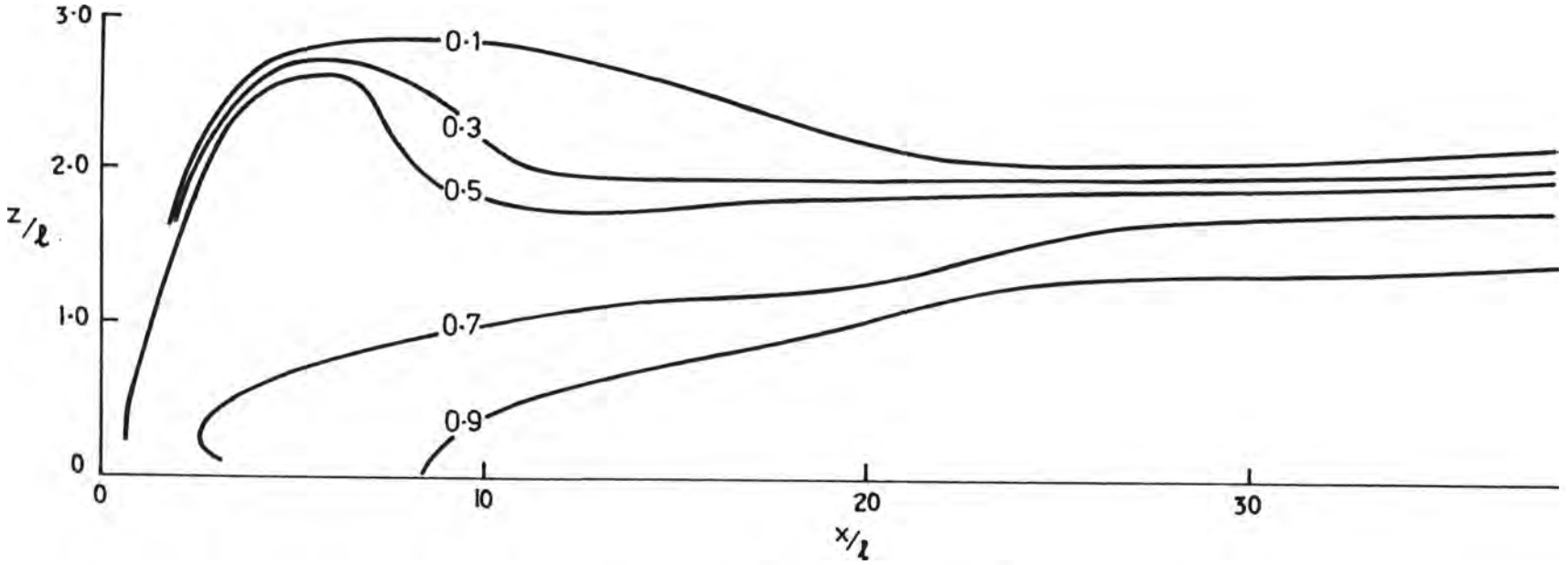

FIGURE 13a: DENSITY STRUCTURE IN TERMS OF y/ℓ AND x/ℓ FOR F_0 = 0.28

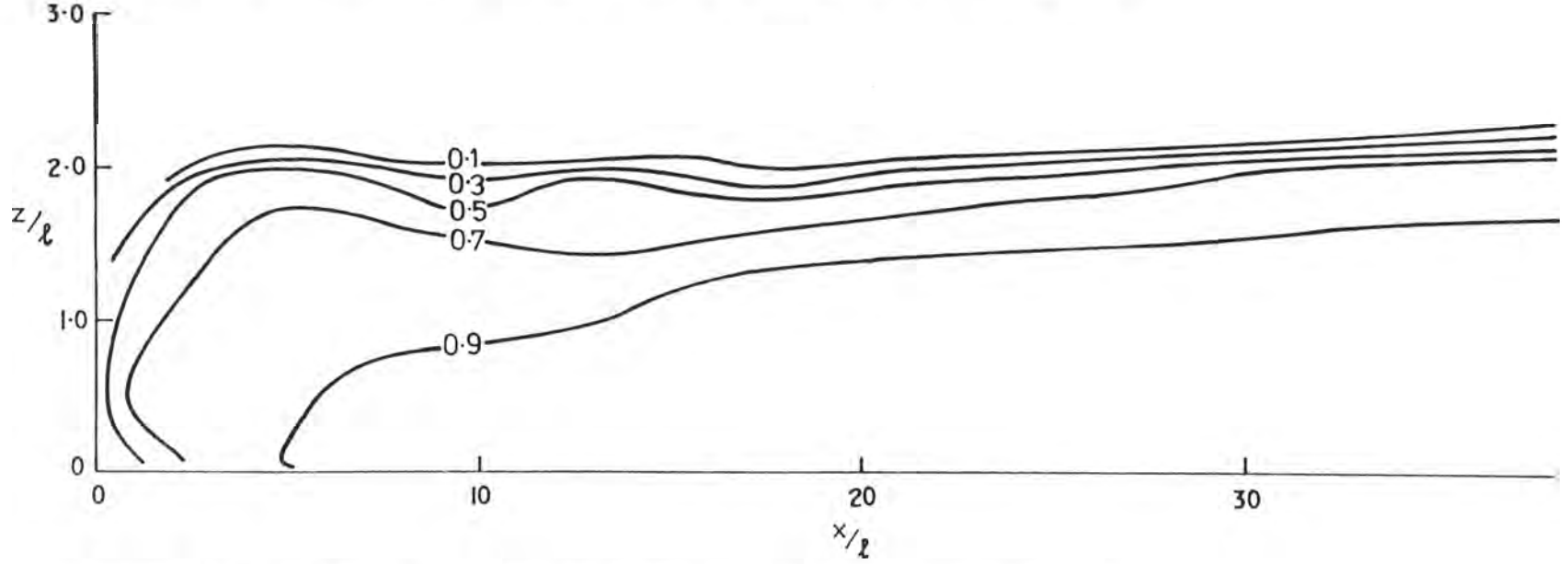

FIGURE 13b: DENSITY STRUCTURE IN TERMS OF y/ℓ AND x/ℓ FOR F_0 = 0.46

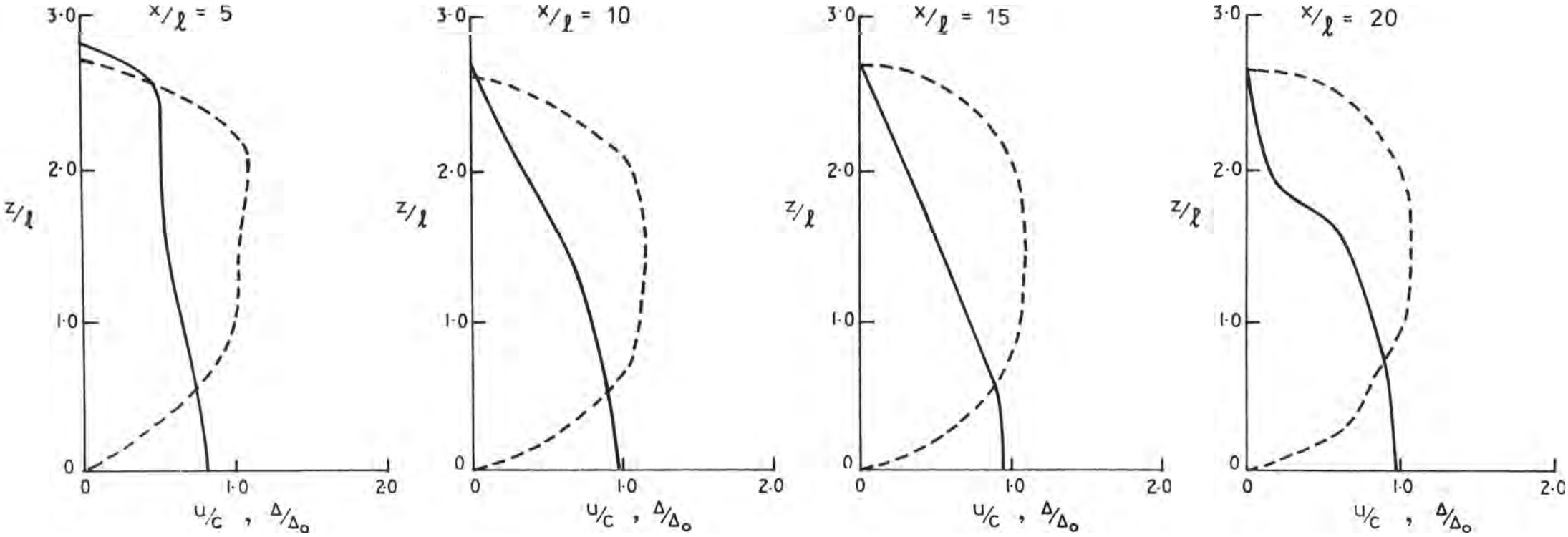

FIGURE 14A: NON-DIMENSIONAL DISTRIBUTIONS OF DENSITY DIFFERENCE AND VELOCITY IN DENSITY CURRENT TRAVELLING BENEATH A DEEP LAYER FOR X/ℓ = 5, 10, 15 AND 20.

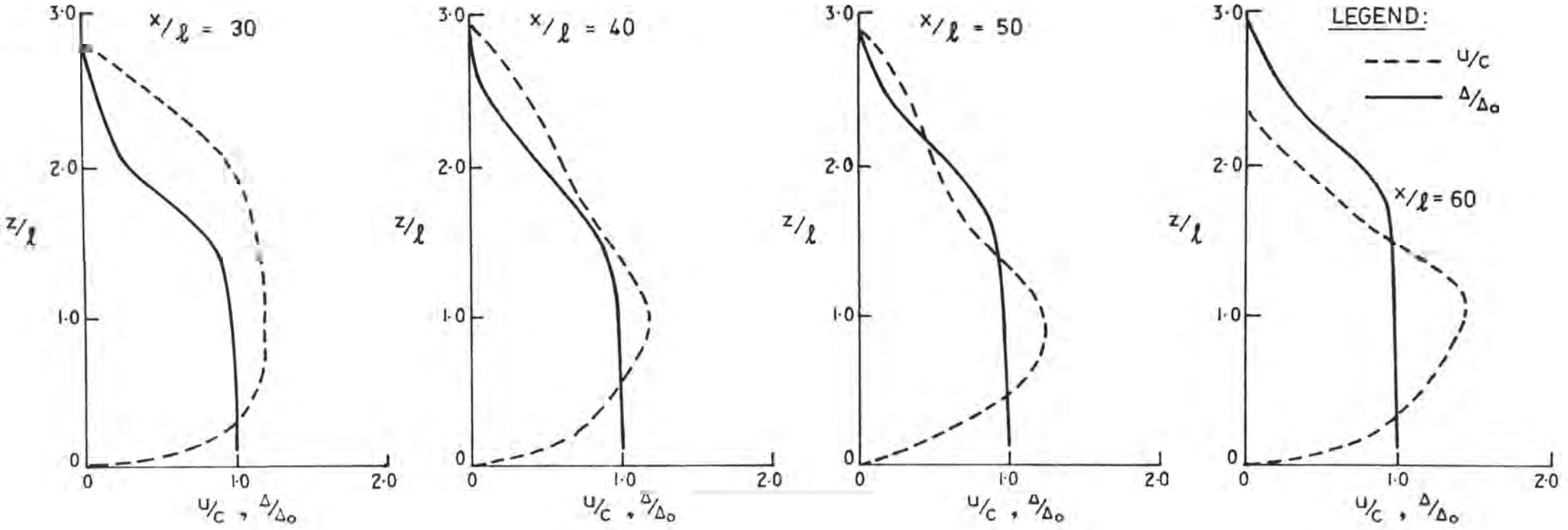

FIGURE 14B: NON-DIMENSIONAL DISTRIBUTIONS OF DENSITY DIFFERENCE AND VELOCITY IN DENSITY CURRENT TRAVELLING BENEATH A DEEP LAYER FOR X/ℓ = 30, 40, 50 AND 60.

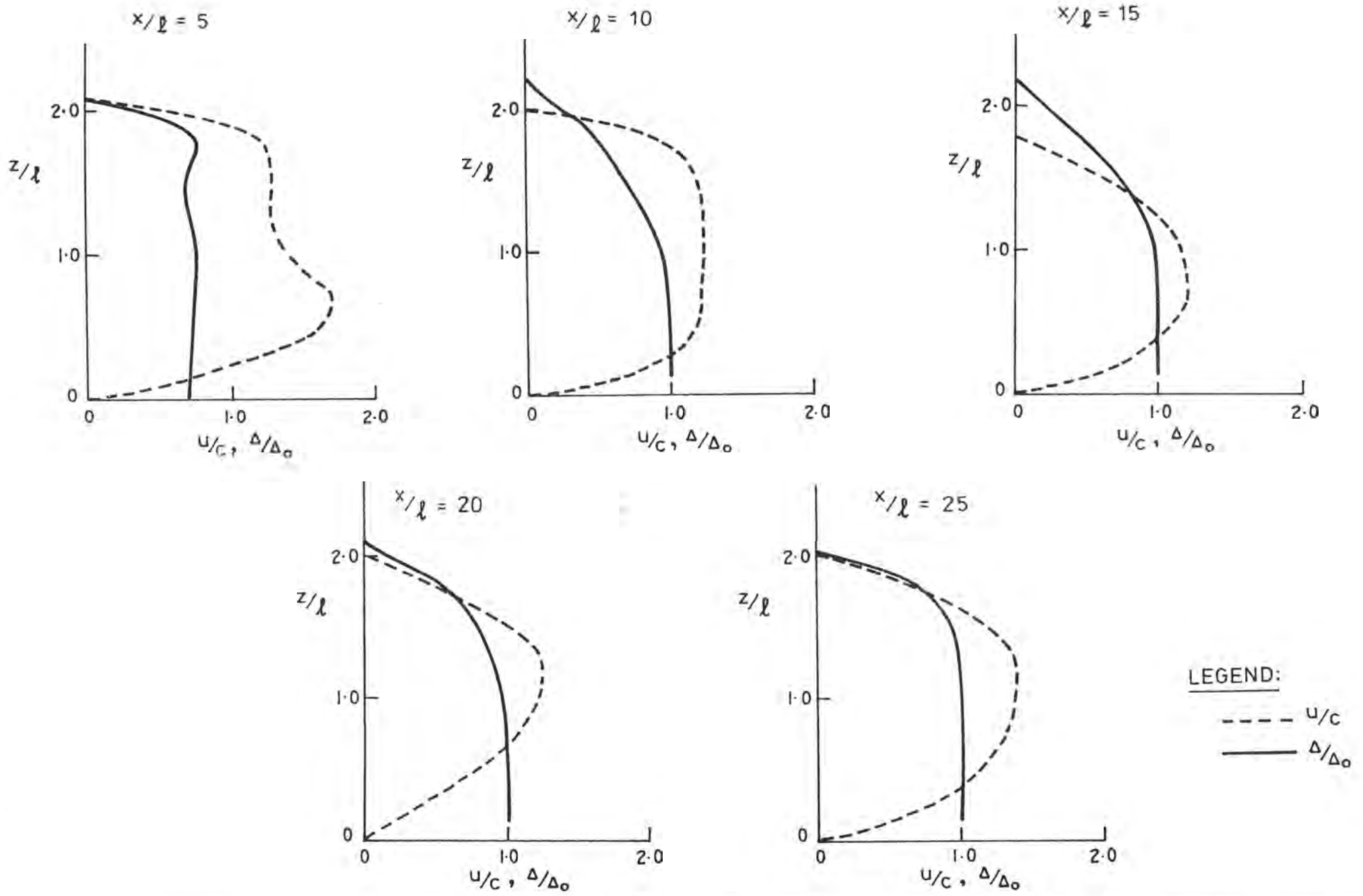

FIGURE 15: NON-DIMENSIONAL DISTRIBUTIONS OF DENSITY DIFFERENCE AND VELOCITY AT VARIOUS VERTICAL SECTIONS IN LOCK EXCHANGE FLOW ($H/\ell = 4.8$)

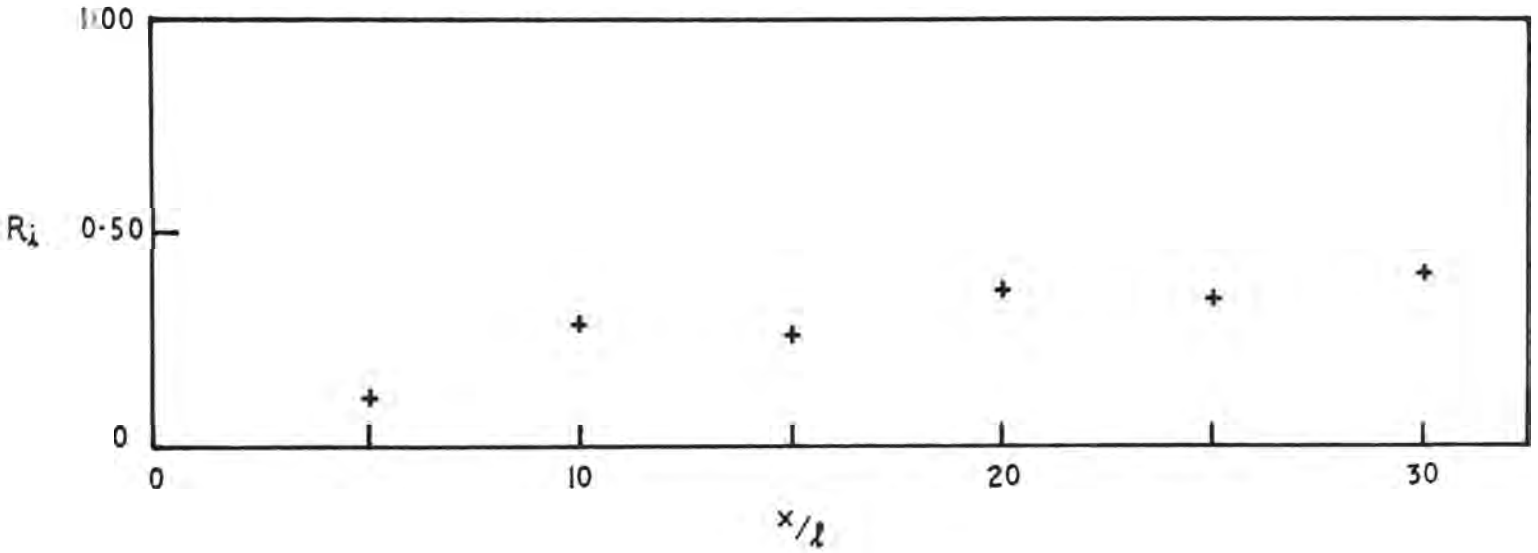

FIGURE 16: GRADIENT RICHARDSON NUMBER OF THE STRATIFIED SHEAR LAYER AS A FUNCTION OF NORMALISED DISTANCE FROM THE HEAD IN A LOCK EXCHANGE EXPERIMENT.

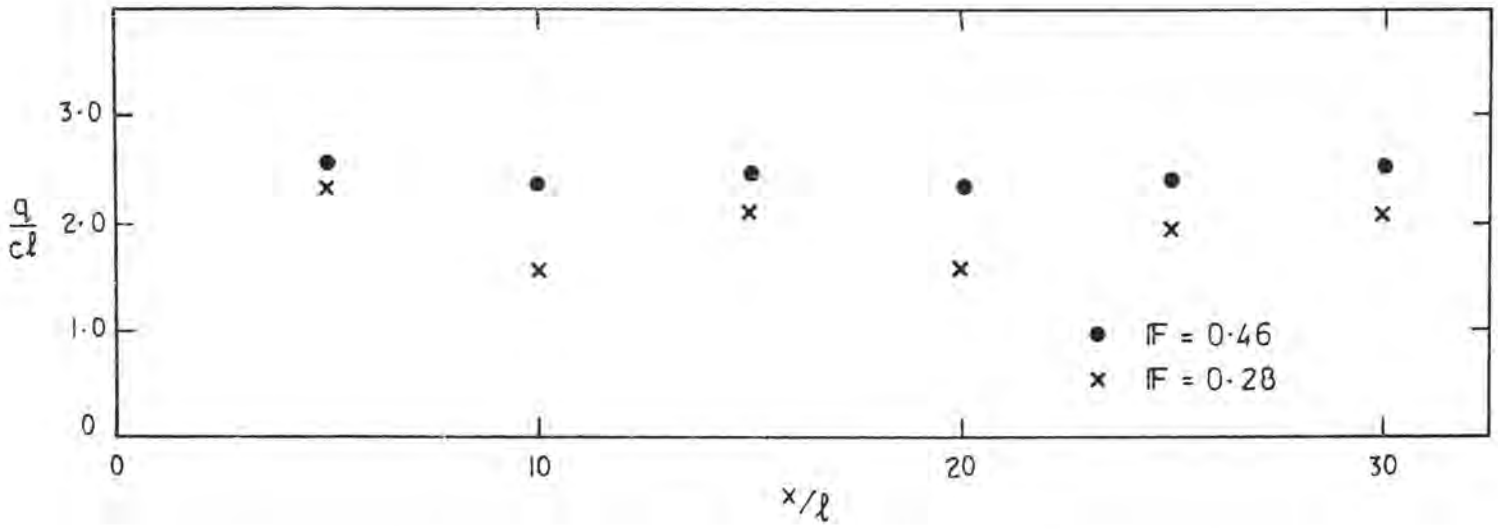

FIGURE 17: NORMALISED VOLUME FLUX AS A FUNCTION OF DISTANCE FROM THE HEAD.

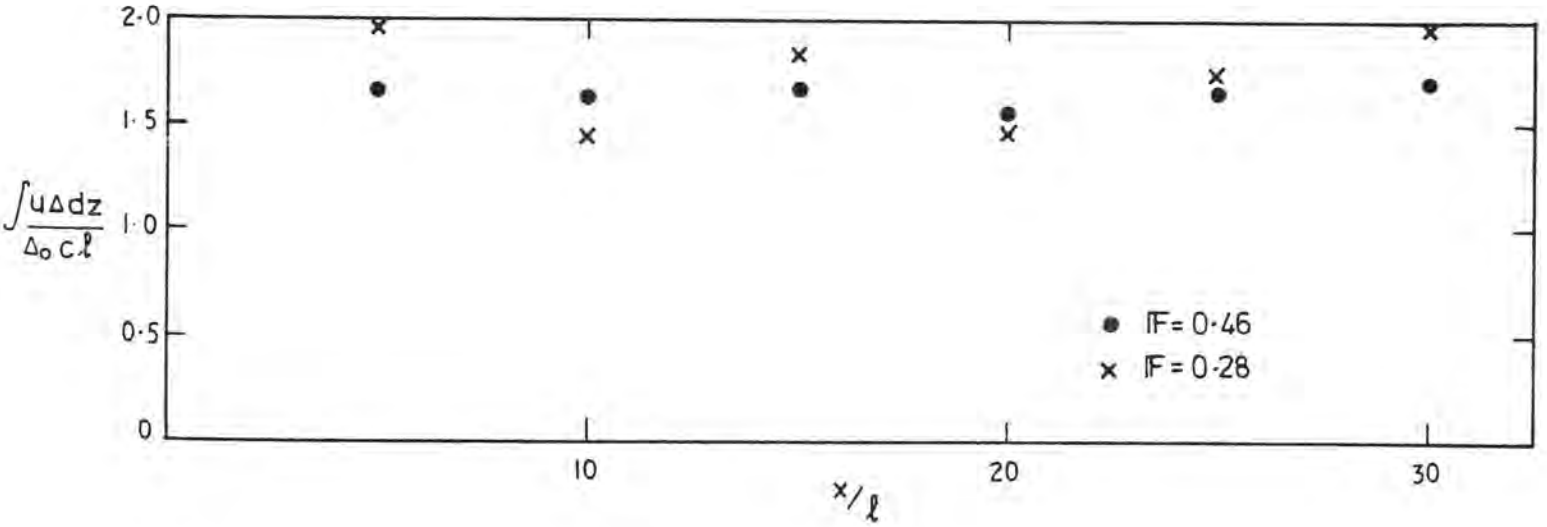

FIGURE 18: NORMALISED FLUX OF DENSITY EXCESS AS A FUNCTION OF DISTANCE FROM THE HEAD.

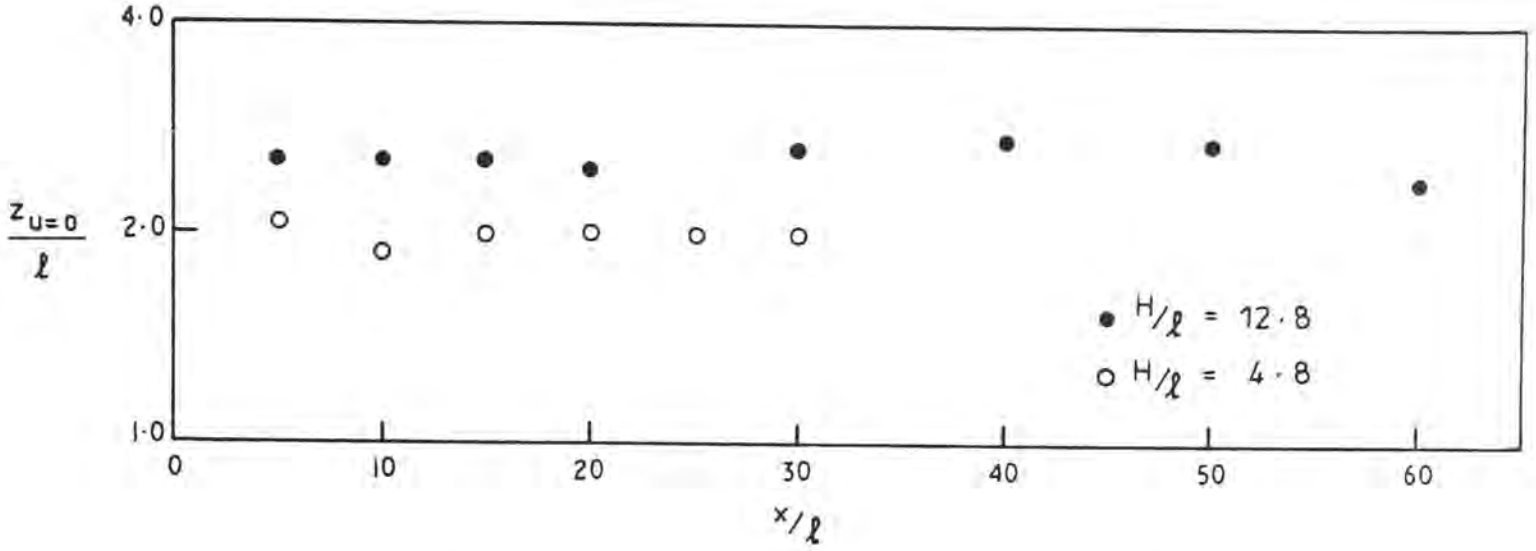

FIGURE 19: LEVEL OF VELOCITY REVERSAL AS A FUNCTION OF DISTANCE FROM THE FRONT.

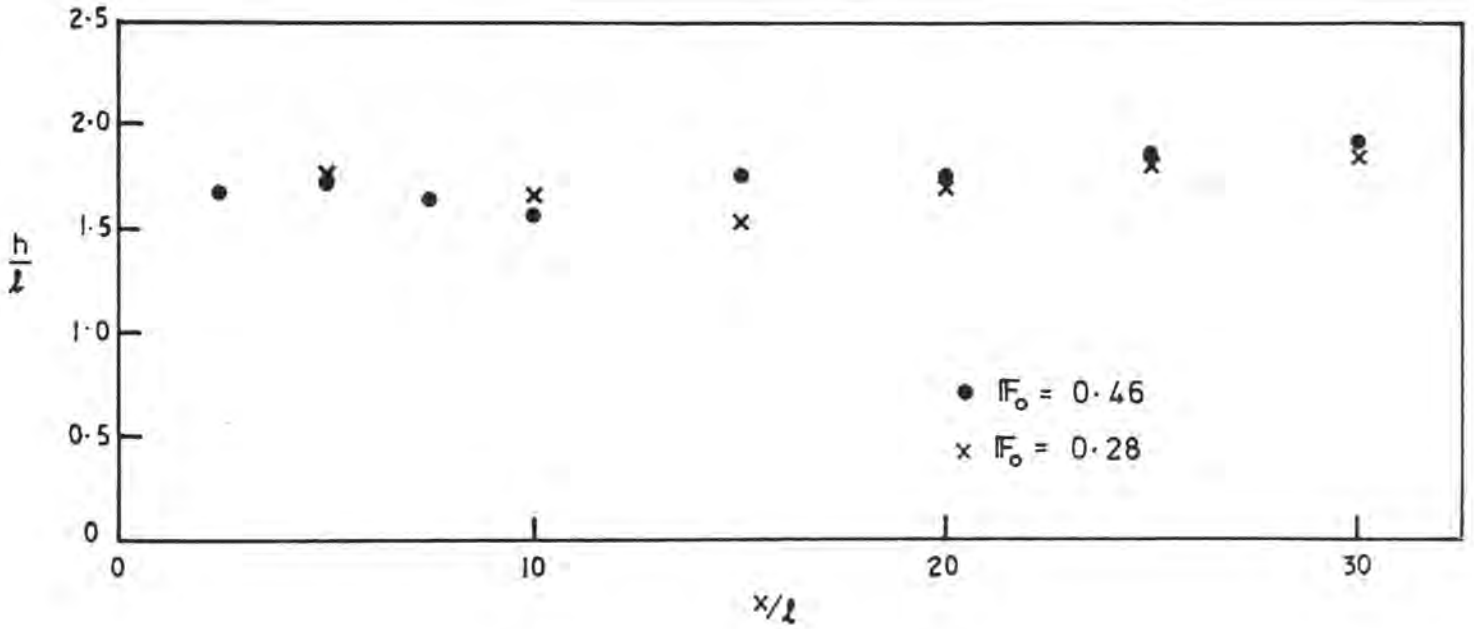

FIGURE 20: HYDRAULIC MEAN LEVEL OF THE INTERFACE AS A FUNCTION OF NORMALISED DISTANCE FROM THE HEAD

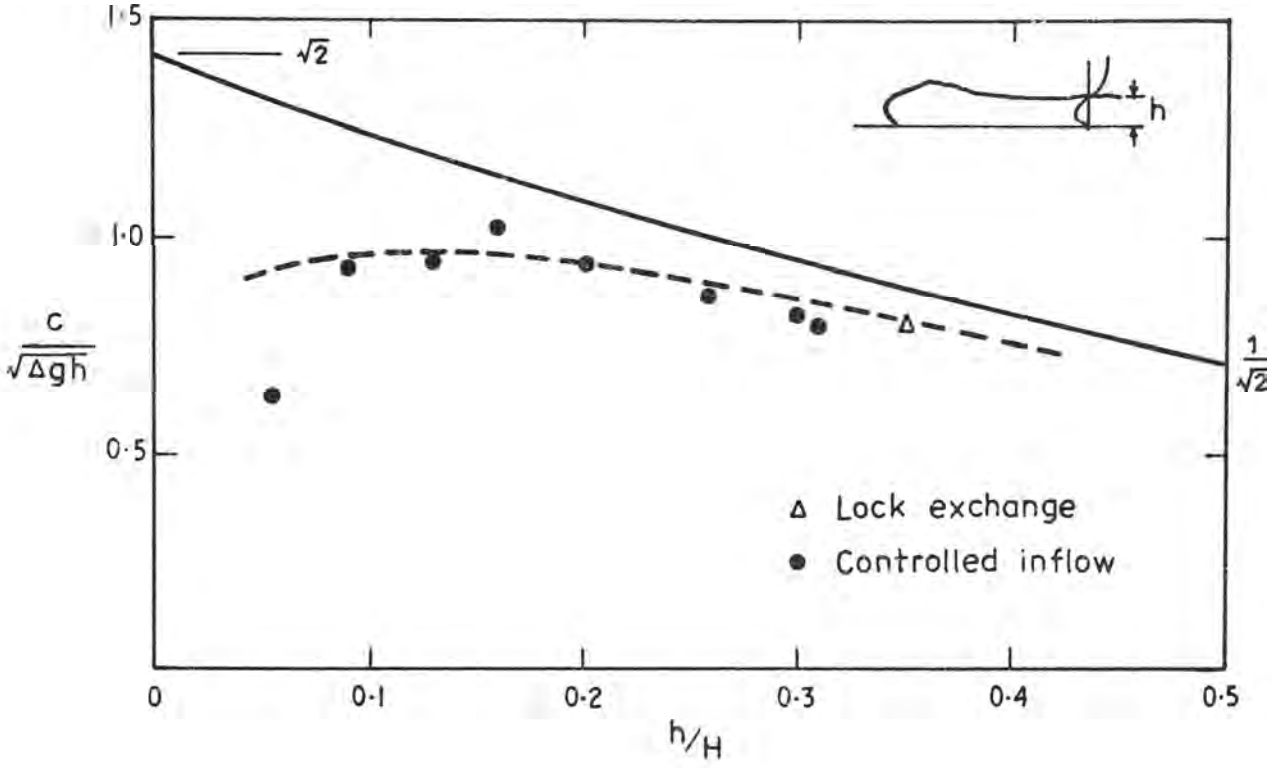

FIGURE 21: FROUDE NO. OF A DENSITY CURRENT FRONT AS A FUNCTION OF THE FRACTIONAL DEPTH.

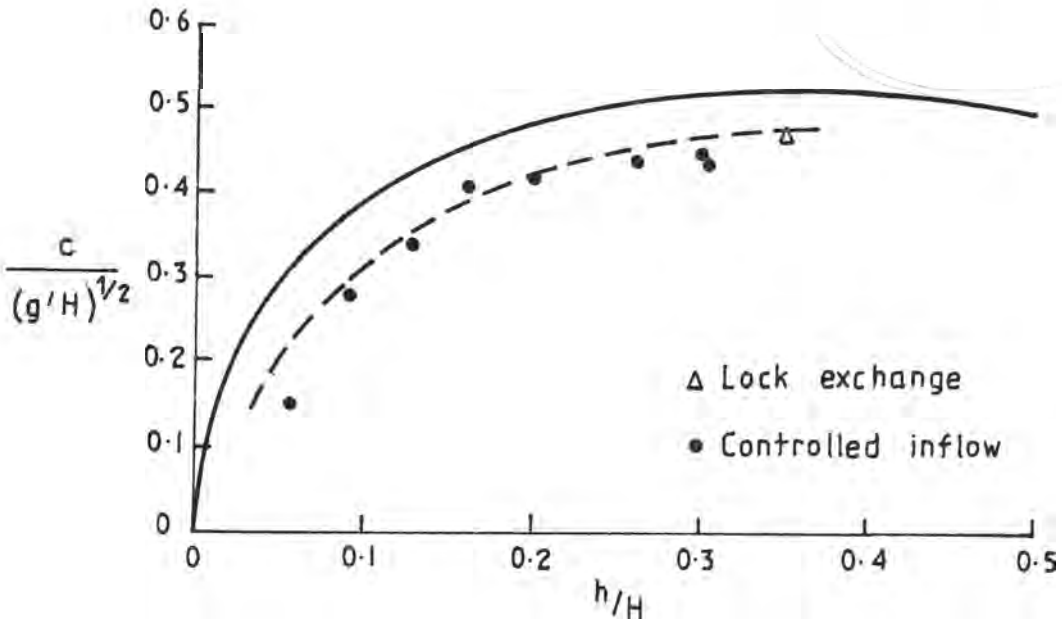

FIGURE 22: NORMALISED CELERITY OF A DENSITY CURRENT FRONT AS A FUNCTION OF THE FRACTIONAL DEPTH.

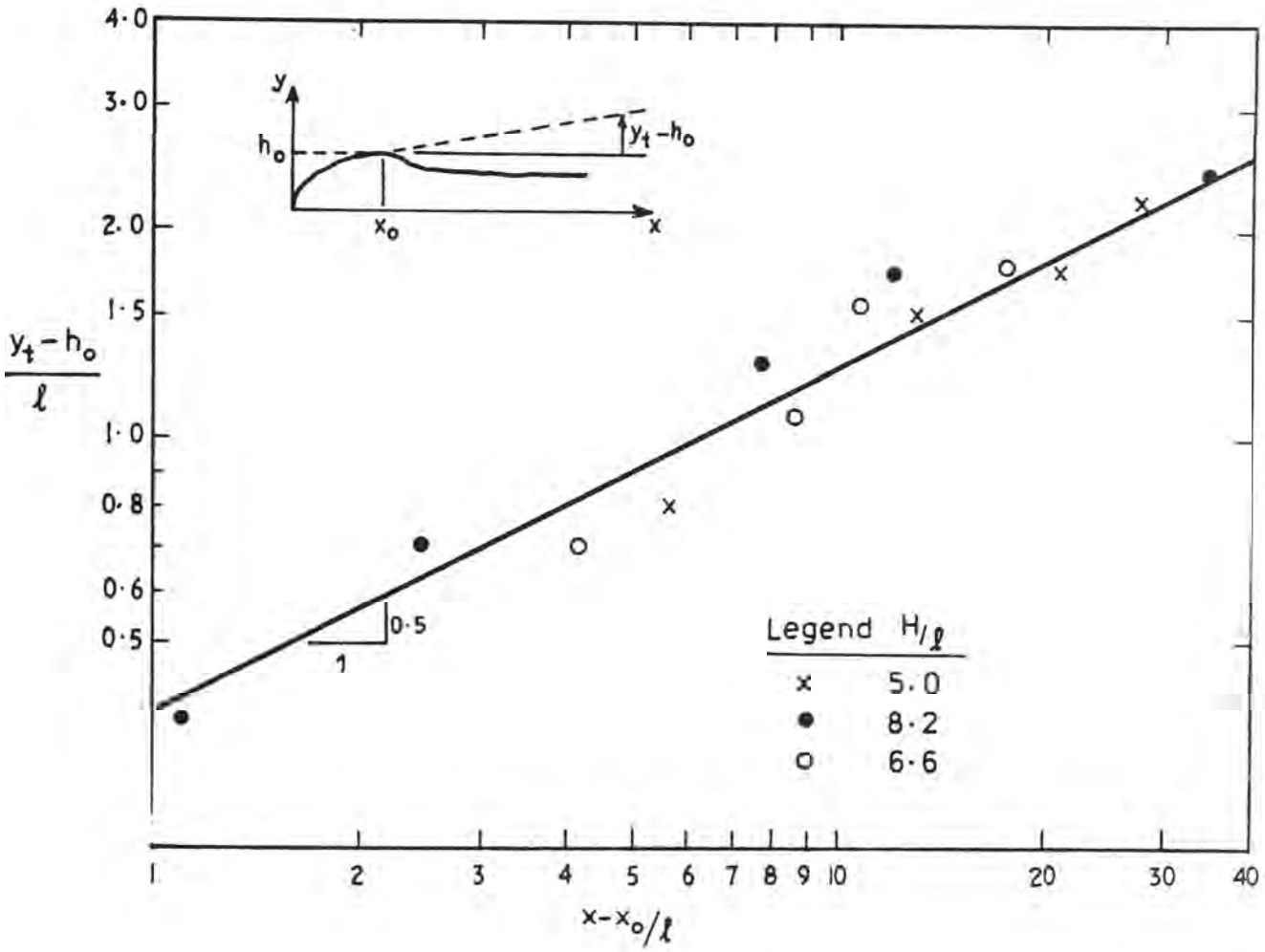

FIGURE 23: GROWTH OF THE WAKE AS A FUNCTION OF DISTANCE FROM THE HEAD OF A DENSITY CURRENT.